NASA Contractor Report 165715

(NASA-CR-165715) VALIDATION OF HELICOPTER NOISE PREDICTION TECHNIQUES Contractor Report, 1979 - 1981 (Bolt, Beranek, and Newman, Inc.) 75 p HC A04/MF A01 CSCL 20A

N81-25768

Unclas
G3/71 26589

Validation of Helicopter Noise Prediction Techniques

George P. Succi

Bolt Beranek and Newman Inc.
Cambridge, MA 02238

Contract No. NAS1-15740
April 1981

National Aeronautics and Space Administration

Langley Research Center
Hampton, VA 23665

VALIDATION OF HELICOPTER NOISE PREDICTION TECHNIQUES

George P. Succi

April 1981

Contract No. NAS1-15740

Prepared by:

Bolt Beranek and Newman Inc.
50 Moulton Street
Cambridge, MA 02138

Prepared for:

National Aeronautics and Space Administration
Langley Research Center
Hampton, VA 23665

TABLE OF CONTENTS

LIST OF FIGURES

LIST OF SYMBOLS

B	Number of blades
c	Sound speed
C	Blade chord
h	Microphone height
L_i	Load vector
M_i	Kinematic Mach vector
M_r	Projection of Mach vector onto the line between a source and observer ($M_r=M_i \cdot \hat{r}_i$)
P_f	Acoustic pressure due to blade forces
P_t	Acoustic pressure due to blade thickness
R	Rotor radius
r	Distance between a source and observer
$\hat{r}_i$	Unit vector directed from source to observer
T	Rotation period
t	Time
TR	Tail rotor harmonic
v	Point volume
V	Helicopter speed
W	Helicopter weight
ρ	Air density
θ	Angular position of the helicopter when it emits sound (retarded position)
ϕ	Angular position of the helicopter when the sound is detected (observed position)
ω	2π times source frequency

1. INTRODUCTION

Growing concern over helicopter external noise levels has recently prompted several countries to propose that noise limits be placed upon the aircraft manufacturer.[1,2] The increasing importance of noise control has placed new emphasis on developing accurate helicopter noise prediction procedures. Most currently used noise prediction techniques are semi-empirical and thus cannot be reliably employed for designs that are significantly different from present helicopter configurations.

Recent methods developed for the prediction of helicopter noise are based wholly on fundamental acoustic principles. This paper describes a study[3] of the analysis developed by Farassat and Nystrom[4], which requires detailed input specifications of the rotor characteristics, operating conditions, and rotor blade surface pressure distribution.

A previous study analyzed certain conditions for the CH-53A and S-76 helicopters.[5] This present study uses measured data for an AH-1G helicopter from the extensive database the Operational Loads Survey (OLS).[6]

The OLS was a comprehensive aerodynamic and structural loads flight test program conducted by Bell Helicopter Textron under U. S. Army sponshorship during the period of Jur 1974 to April 1976. A heavily instrumented main rotor was flight tested through a wide range of operating conditions. One objective of this investigation was to record the rotor's aerodynamic environment and to record on the ground simultaneously acoustic time histories of the operation. To date, analysis of the aerodynamic data recorded has been directed toward describing such rotor aerodynamic behavior as retreating blade stall, normal force variation and distribution, angle of attack variation, and blade/wake interaction.[7]

Six level flight flyovers ranging from 20 m/sec to 67 m/sec were chosen for the study from the OLS database. Flights are at a nominal altitude of 91 m (300 ft). The blade-loading data were digitized and made available in one-degree increments for computer processing. The data were reduced into C_p and C_N (similar to C_L) values and plotted. A sample C_N three-dimensional plot is shown in Fig. 1. From 30 to 50 revolutions were provided to represent each condition.

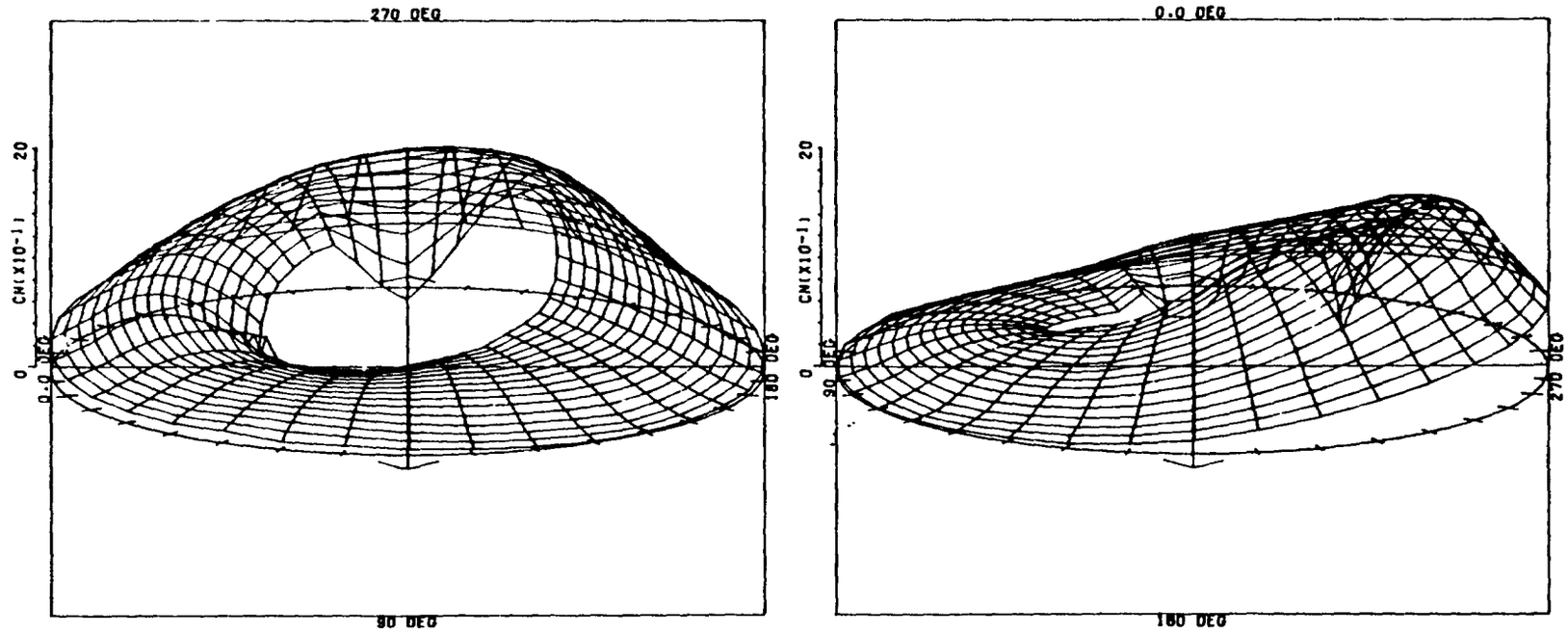

SIDE VIEW

FRONT VIEW

FIG. 1. THREE-DIMENSIONAL C_N PLOT FOR 67 M/SEC AIRSPEED IN LEVEL FLIGHT

These load data were then integrated into a Farassat/Nystrom noise prediction computer program.[3,4] Noise predictions based on the measured blade loads were compared to the measured noise. An evaluation of predictions was made for several flight velocities and helicopter locations. A noise prediction based on theoretical blade loads was also made and compared to the predictions based on the measured loads. This second technique was used to determine if accurate helicopter noise predictions could be made using only theoretical quantities.

2. TEST EQUIPMENT*

2.1 Test Helicopter

The OLS program required complex instrumentation to be mounted on a standard helicopter. All modifications were made in low load or nonstructural areas to ensure that the basic structural integrity of the airframe was not compromised.

The test helicopter, a bailed U. S. Army AH-1G helicopter, and instrumented main rotor are shown in Fig. 2 (the tail rotor was not instrumented). In addition to the standard equipment in the helicopter, the following items were installed: 1) A set of modified main rotor blades instrumented with absolute pressure transducers; 2) a 28-track AR-728 tape recorder, a stationary FM multiplex, and a telemetry (TM) transmitter; 3) a rotating FM frequency-division multiplex system mounted to the hub trunnion; 4) A nose boom mounted forward of the ship for airspeed and fuselage attitude measurement. Numerous other transducers included hot-wire sensors, surface flow sensors and accelerometers mounted on the blades, and accelerometers and microphones mounted on the fuselage. Fuselage pitch attitude and hub flapping angles were used to estimate the position of the main rotor tip path plane.

2.2 Modified Main Rotor Blades

Two main rotor blades were modified as shown in Fig. 3, with a 3.302-mm constant thickness fairings (gloves) bonded to the upper and lower surfaces to provide a smooth, contoured, accurate airfoil surface on which transducers could be mounted.

*The section on test equipment was written by John Breiger of Bell Helicopter Textron.

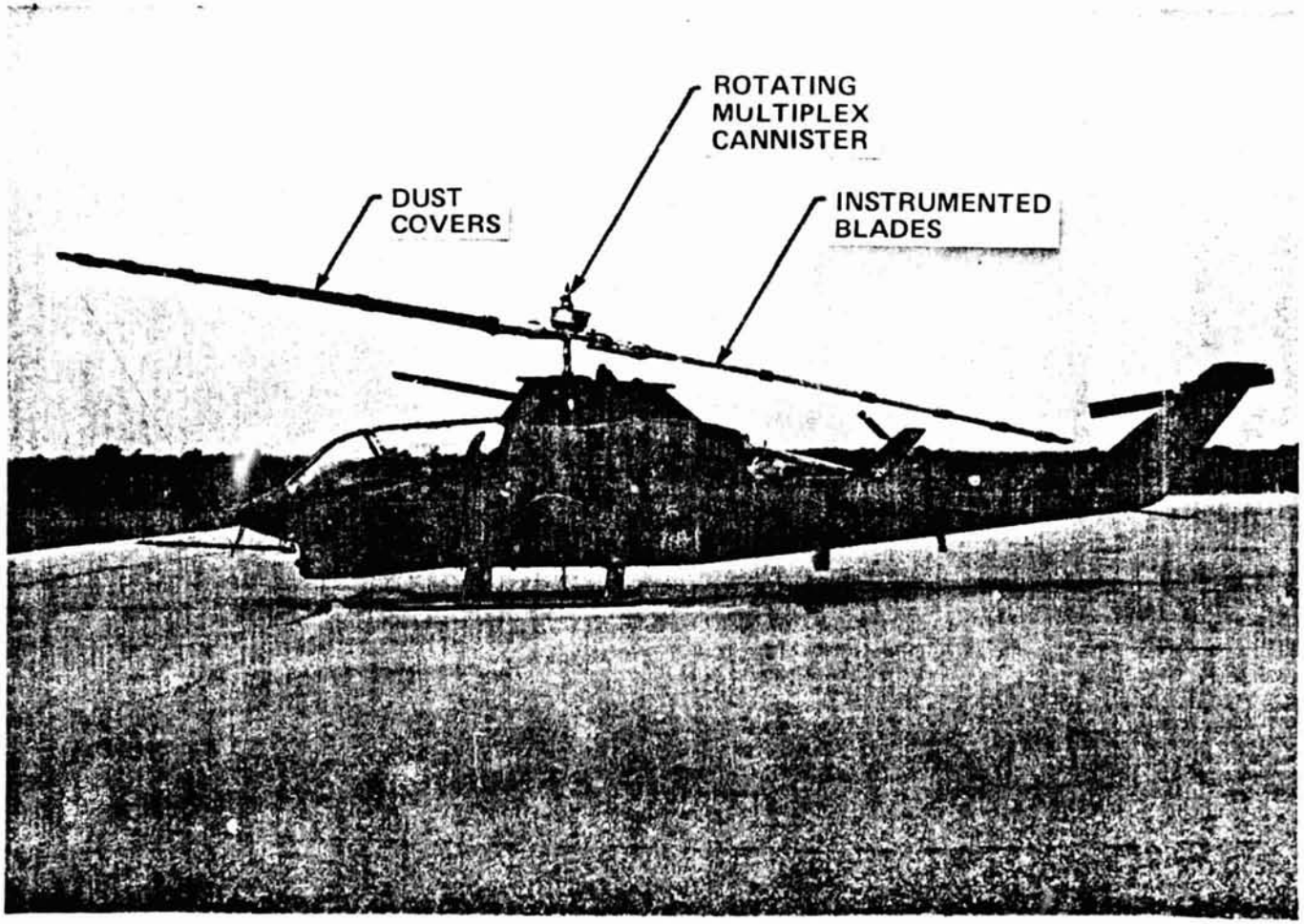

FIG. 2. AH-1G TEST HELICOPTER.

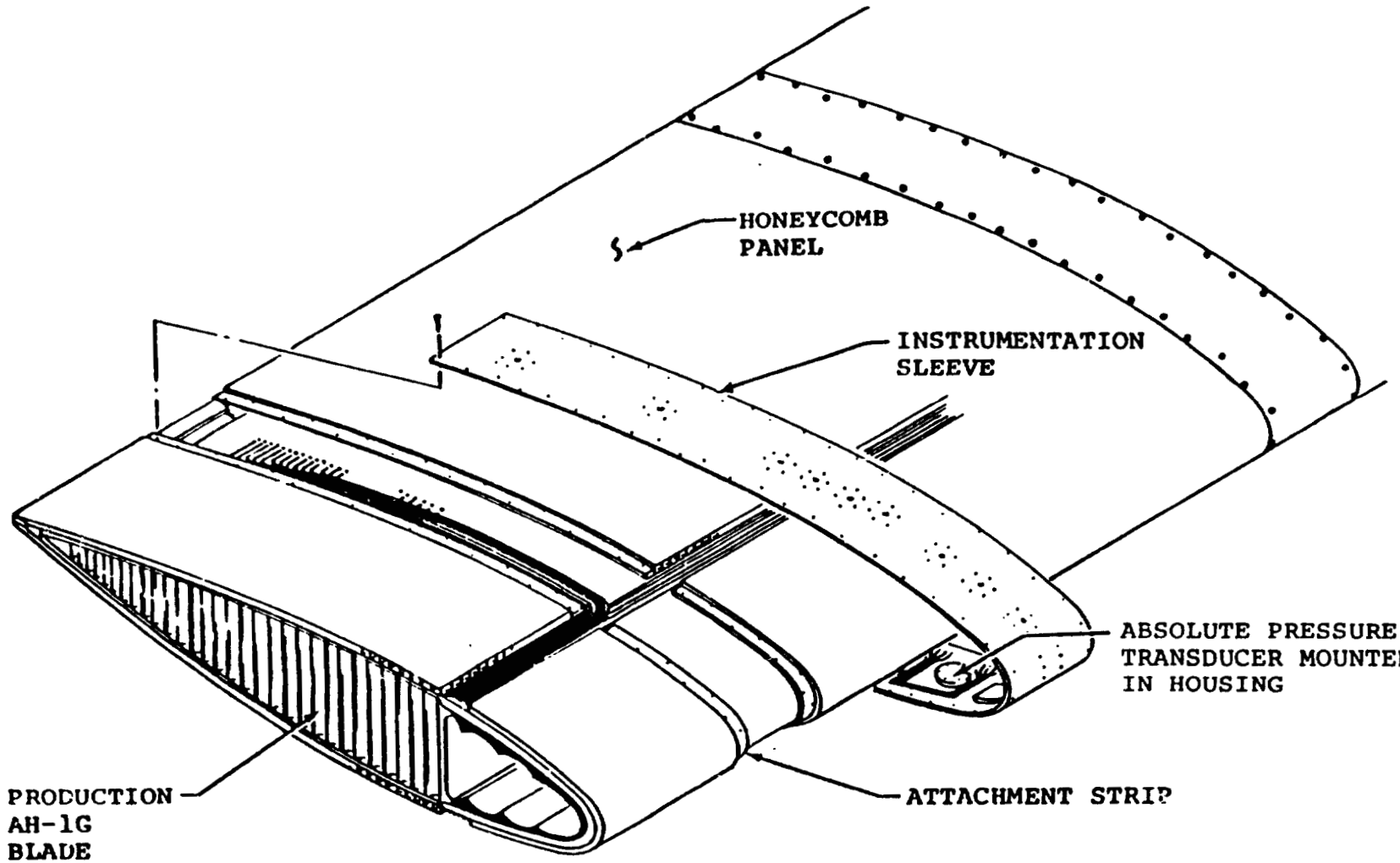

FIG. 3. ROTOR BLADE CONSTRUCTION AND INSTRUMENTATION INSTALLATION

The blade natural frequencies were kept similar to the production blade by removing a portion of the midspan weight and reducing the tip weight. Centrifugal force, mass balance, and blade weight were maintained within design limits.

The glove consisted of stretch-formed aluminum leading edge strips and thin fiberglass afterbody skins supported by a Nomex honeycomb core. The panels and strips were omitted at the five radial stations requiring instrumentation. The instrumentation was housed in 10-cm-wide rolled aluminum sleeves that wrap around the blade at those stations. The trailing edge was extended 3.8 cm beyond the original edge to a thickness of 2.5 mm. The glove thickness and chord extension resulted in a 0.4% increase in airfoil thickness ratio.

2.3 Blade Instrumentation

One blade contained 110 Kulite absolute pressure transducers to measure static pressures. They were on the upper and lower surfaces from the leading edge to the trailing edge at 40, 60, 75, 86.4 and 95.5% radii. At a given station, the chordwise distribution of transducers on the upper and lower blade surfaces was the same. Pressure transducers were concentrated at the outboard radial stations to record the major pressure peaks and the important shock formations.

2.4 Acoustics Acquisition System

Microphones were both mounted on the helicopter and based on the ground during much of the survey. This study uses only that data taken using the ground microphones.

The ground-based acoustic system included three tripod-mounted B&K 1-in. micorphones at standing ear level located 500 ft apart on a line perpendicular to the flight path. The microphone data were recorded FM at 30 IPS giving a flat frequency response from 0 to 10,000 Hz. The 14-track AR-200 tape recorder also recorded azimuth and elevation signals from a prototype optical aircraft tracker, a voice track, and a telemetered level code signal from the aircraft to correlate aircraft time code with ground-based time code.

3. VALIDATION OF PREDICTION TECHNIQUES

3.1 Acoustic Prediction Method

The noise field may be deduced from both the shape and motion of the rotor and from the azimuthal and radial variations of the aerodynamic loads. The relation between rotor conditions and the noise field is expressed as an integral over the blade surface conditions, with account taken for both the motion between source and observer and the finite sound propagation time across the rotor disk plane. The set of relations that generate the sound field from the given rotor condition is termed "the acoustic calculation"[9] and is embodied in the computer program of Farassat and Nystrom.[4] This analysis is based on a solution of the Ffowcs Williams-Hawkings equation and includes terms that account for both the thickness and loading components of the rotational noise. Thickness noise is due to the finite size of the rotor. Loading noise is due to the forces developed by the rotor. Loading noise is further classified as steady and unsteady loading noise, where unsteady loading noise is due to fluctuations in the rotor forces.

There are two types of information necessary for the acoustic calculations: blade geometry and blade loads. The blade geometry includes a description of the rotor shape and motion. The shape description includes the number of blades, airfoil section properties, blade chord and blade twist The motion description includes the distance between source and observer, forward velocity of the rotor hub, the rotor rotation rate, the rotor attitude, and the azimuthal variation of the blade pitching and flapping. This information is available from the previously mentioned OLS database. In all cases, the mean experimental values of the conditions are used.

Blade-loading information is obtained from both measurement and theory. The OLS base provides measured absolute pressure data in both radial and chordwise distributions. Of special importance acoustically is adequate pressure sensing on the leading edge and near the blade tip. A computer program is used to obtain the theoretical blade loading. Various methods are available for calculating these loadings, including blade element momentum analysis and vortex theories. The analysis chosen for this study is one developed by Scully.[10] This program assumes section characteristics for the blade elements. The input includes the blade shape, rotor velocity, RPM, and desired thrust coefficient. Calculations are carried out by altering the azimuthal variation of the blade root pitch until the desired thrust coefficient is obtained.

To calculate blade loads on a helicopter rotor, the influence of the wake is of primary importance. Scully provides the user with several options including wake deformation and alteration of the vortex core (bursting). He finds, however, that the more complex models of the wake structure yield no better results than those from a distribution of vortices on a rigid helical surface. With this result in mind, the simplest model for the aerodynamic calculation was chosen, that of a rigid skewed helical vortex sheet. The lift per unit radius is tabulated at 6 radial locations in 15-degree increments. Uniform chordwise variation in lift is assumed.

Prior to presenting the results, one must include an approximate correction for the influence of the ground because all measurements were made with a microphone mounted 1.2 m above a mowed grass surface. The ground influence is approximated by assuming that it is a boundary of infinite impedance, i.e., it has a reflection coefficient of one. This is difficult to prove as there are no measurements of ground impedance in the 10-Hz range. (Note that the blade passing frequency is 10.8 Hz.) However, Embleton's[11] measurements in the 100-Hz to 1-kHz range indicate that the reflection coefficient tends to one as the frequency is reduced to zero; hence, the choice of R = 1.

The helicopter position is identified by an angle relative to the ground observer. At 0°, the helicopter is approaching from the horizon; at 90° it is overhead; at angles greater than 90°, the helicopter is receding from the observer. Moreover, the helicopter's position when it emits the sound, θ, is distinguished from its position when the sound is received, ϕ. This distinction is necessary because the vehicle moves during the time it takes for the sound to reach the observer.

3.2 Review of the Source Terms

To understand the computations, it is useful first to review the basic expressions for sound generation from a moving body. The simplest expressions are those for sound generation from a compact source. Though these expressions are not used in the Farassat/Nystrom program, they have been shown to be equivalent.[9,12]

Of particular interest is the relative influence of the magnitude of the loading and thickness source terms, L and V, and the fluctuating geometrical arrangements between the source and observer.

In the following discussion, the concept of a point force source and point volume source is introduced. The first successful prediction of rotor noise was due to Gutin using an expression for sound from a stationary point force.[13] Gutin replaced the blade forces by a distribution of oscillating forces in the propeller disk. He then used a solution for the acoustic field of a stationary point force and the superposition principle to calculate the harmonics of the propeller noise. A similar model is used here to motivate the discussion of the validation test. The rotor blade can be replaced by an array of points where each point has the force and volume of the associated section of the rotor blade. The time domain expression for the pressure field due to these forces is given. For any particular location of the helicopter rotor and observer, reference to these point force equations aids the interpretation of the results.

Consider the farfield expression for the loading noise from a compact source[12,14]

$$p_f = \left[\frac{1}{4\pi r}\frac{1}{(1-M_r)^2}\left[\left(\frac{\hat{r}_i}{c}\cdot\frac{\partial L_i}{\partial t}\right) + \frac{L_i\cdot\hat{r}_i}{(1-M_r)}\left(\frac{\hat{r}_i}{c}\cdot\frac{\partial M_i}{\partial t}\right)\right]\right], \qquad (1)$$

where p_f is the acoustic pressure due to blade loads, r is the distance between the source and observer, t is the time, $\hat{r}_i$ is the unit vector in the direction from source to observer, L_i is the force vector, M_i is the Mach number based on the source velocity, $M_r = M_i \cdot \hat{r}_i$. Braces indicate the computation is done at the retarded time.

The calculated pressure field depends on both the force, L_i, and the geometric relations between the source and observer contained in the terms: r_i, M_r, and M_i. For observations near the disk plane, the calculation of the noise is dominated by the time dependent fluctuations in the geometric parameters. Here, the greatest effects are due to fluctuations in the term $(1-M_r)$, which appears in the denominator. Even a simple estimate of the rotor forces yields a good noise prediction.

However, when the observer is on the rotor axis, where the fluctuations in the geometric parameters are minimal, the calculated pressure field is dominated by the unsteady loading term, $\partial L_i/\partial t$. Hence, to calculate the noise accurately when

the helicopter is overhead, a very accurate measure of the blade loading is needed. Much of the discussion in the paper concerns how accurate an input of rotor loads is needed for an accurate prediction of the rotor noise.

A similar expression can also be written for the thickness noise of a compact source:[12]

$$P_t = \rho v \left[\frac{1}{1-M_r} \frac{\partial}{\partial t} \left[\frac{1}{1-M_r} \frac{\partial}{\partial t} \left(\frac{1}{r(1-M_r)} \right) \right] \right] \qquad (2)$$

where p_t is the acoustic pressure due to blade thickness, v is the volume of the moving source, and ρ is the air density. When the relative velocity between the source and observer is zero (M_r=0), no noise is emitted; hence, thickness noise is minimal for observations made on the rotor axis because the relative velocity between the source and observed is approximately zero.

One asymmetry that appears in both the measured and predicted noise is the asymmetry in disk plane observations. In the Bell experiment, a disk plane observation occurs when the helicopter is on the horizon. The asymmetry is determined by whether the helicopter is approaching or receding from the observer. This asymmetry is due to the forward motion of the helicopter. In particular, it is due to the variation in M_r, the Mach number based on the relative velocity between the blade element source and the observer. When the helicopter approaches the observer, the maximum M_r occurs at the tip of the advancing blade and is approximately equal to the sum of the Mach numbers based on air speed and tip speed. When the helicopter recedes from the observer, the maximum M_r occurs at the tip of the retreating blade and is approximately equal to the difference between the Mach numbers based on air speed and tip speed. Reference to Eqs. (1 and 2) shows that this asymmetry in M_r results in an asymmetry in the maximum pressure for both thickness and loading noise.

A word of caution is in order. The discontinuity of the equations at $M_r = 1$ is an artifact due to the assumption of a compact source. This discontinuity disappears when the finite extent of the source is considered. Proper account of the finite extent of the source is made in the Farassat/Nystrom program.

A further caution is needed concerning the Farassat/Nystrom acoustic program. In the acoustic program, the primary reference line is the chord line. However, the Farassat/Nystrom program permits the programmer to use a simplified procedure, which includes only forces that are perpendicular to the chord. All forces that manifest themselves in the surface pressure distribution can be included in the Farassat/Nystrom program, even those that result in forces parallel to the chord. In this paper, only forces perpendicular to the chord line are included so as to simplify the calculation procedure. This does allow a possibility for an avoidable error; when $\hat{r}_1$ is parallel to the chordline, the procedures used in this paper give zero loading noise.

3.3 Loading Noise Calculations

The first acoustic computation deals with the details of the experimental loads. The problem is to determine the best value of experimental loads to use as an input into the acoustic calculation. In particular, the problem is to determine whether it is better to use an average of 50 cycles to describe accurately the mean properties of the signal, or to use a single cycle "snapshot" of the load field. Figure 4 shows the predicted loading noise based on both the instantaneous and average measured loads. (The effect of blade thickness on the predicted noise signature is not shown in Fig. 4.) The most important difference is the pressure spike on the advancing blade. This spike is greater for the "snapshot" of the blade loads. This difference is due to slight variations in the locus of the blade vortex interaction. Though the variation from one cycle to the next is small, the variation between a single cycle and an average of many cycles is great enough to affect the acoustic calculations. The effect of small shifts in the azimuthal location of the pressure spike is such that the average pulse is somewhat smaller than the instantaneous one. This difference reduces the calculated acoustical signal. Henceforth, the single cycle of load data is used because it more accurately represents the height of the blade vortex interaction spike.

The next computation concerns details of the calculated loads. The problem is to find out how accurate a description of the load distribution is necessary in order to make a reasonable computation. The simplest load distribution possible is to compute an average pressure drop,

$$\Delta P = W/(B \cdot C \cdot R) \quad , \tag{3}$$

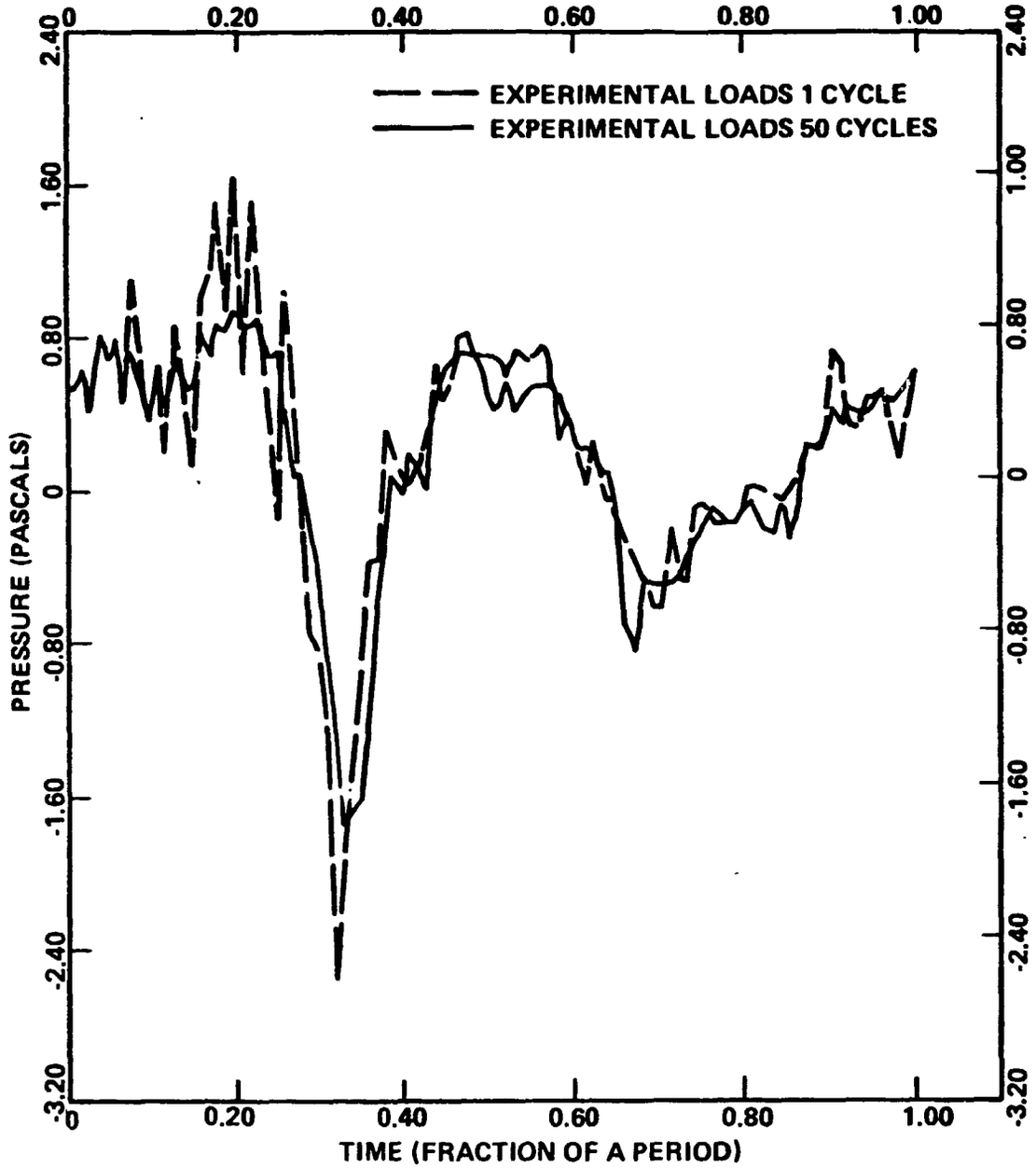

FIG. 4. CALCULATED ACOUSTIC LOADING NOISE SIGNATURE
(V=41 M/S, $\theta \approx 140^{o}$)

where W is the helicopter weight, B is the number of blades, C is the rotor chord, and R is the span; i.e., ΔP is the weight divided by the blade area. For comparison, the signature calculated from the theoretical load data and experimental load is also given. Figure 5 shows the predicted loading noise based on the three different representations of the blade loads. (Again, influence of blade thickness is not shown in Fig. 5.)

In Fig. 5, the computation is done at the $\theta = 8.8°$ point (i.e., the observer is almost in the disk plane). Here the pressure signature from the simple uniform load model is nearly the same as that from the vortex wake calculation of the loads. The reason is that the fluctuating sound field is due partly to the load fluctuations and partly to the motion of the blade. Even a simple calculation of the load field yields good results in the disk plane.

The most important feature that is not modeled correctly by the uniform load assumption is the pressure spike at 30% of the blade period. This spike depends on the detailed character of the blade loads. It is due to an increase in the blade load due to a blade vortex interaction. Reference to Eq. (2) shows that this alters the calculated load noise by increasing the steady load term L_i and also by introducing the unsteady load term $\partial L_i/\partial t$. This pressure spike appears in the predicted noise signature based on the experimental loads and the loads calculated from Scully's vortex wake model (the theoretical loads).

Figure 5 also shows the similarities between the signature calculated from the theoretical and measured loads. Both have a pressure spike at approximately the same time. However, the magnitude of this spike is different. This discrepancy becomes more critical as the vehicle passes overhead. When the vehicle is overhead, unsteady load fluctuations dominate the noise signature from the main rotor. Hence, a more accurate calculation of the loads is needed. A further example of this error is indicated in Fig. 6.

In Fig. 6, the first harmonic level of the "loading noise" is calculated at several observation angles for two blade load inputs. In one case, the experimental loads are used; in the other case, the theoretical loads are used. At shallow observation angles, the two predictions agree. The predictions agree because the noise signature is strongly influenced by blade motion. Overhead, the two predictions disagree. The

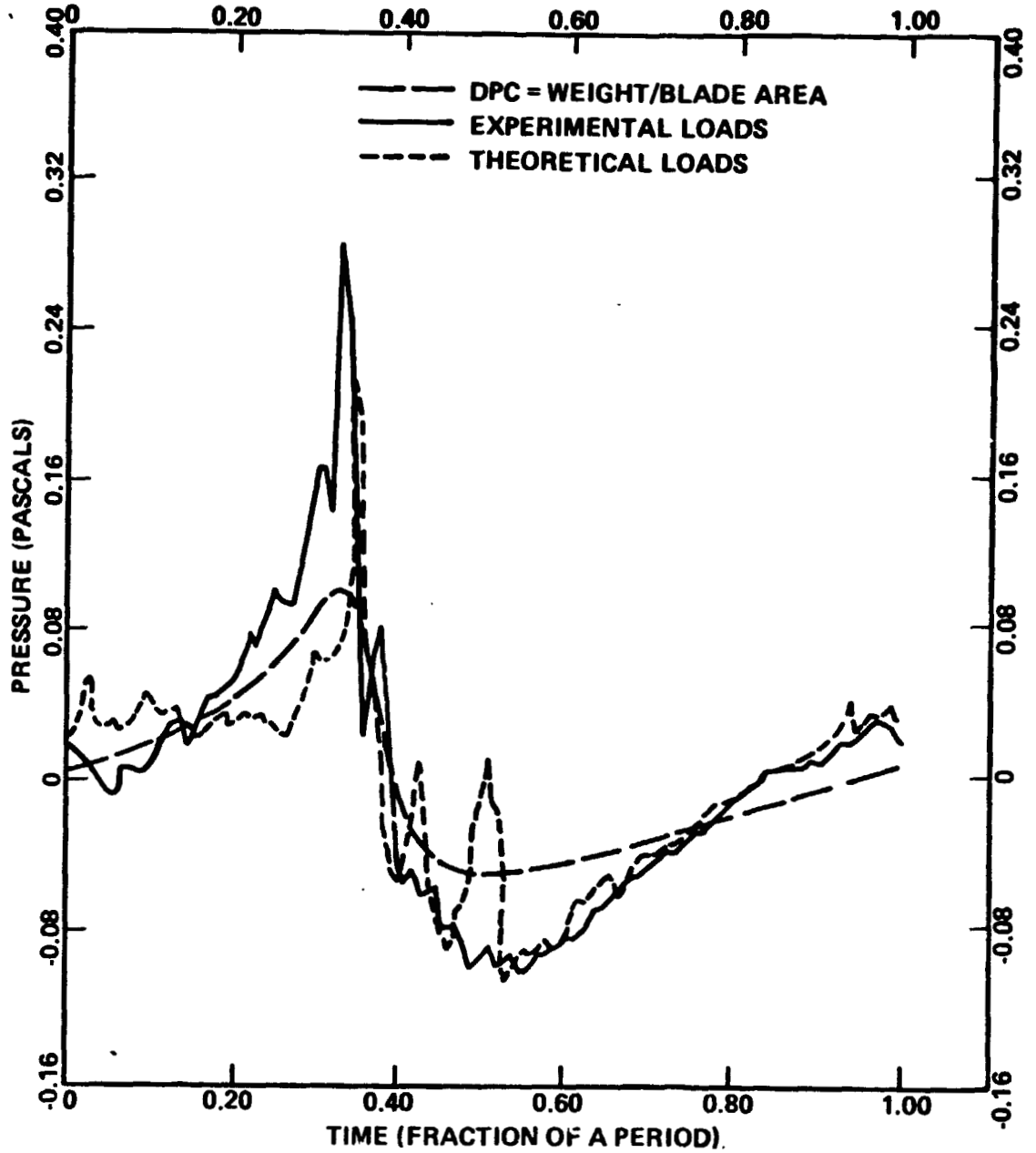

FIG. 5. CALCULATED ACOUSTIC LOADING NOISE SIGNATURE
(V=41 M/S, $\theta \simeq 9^{o}$)

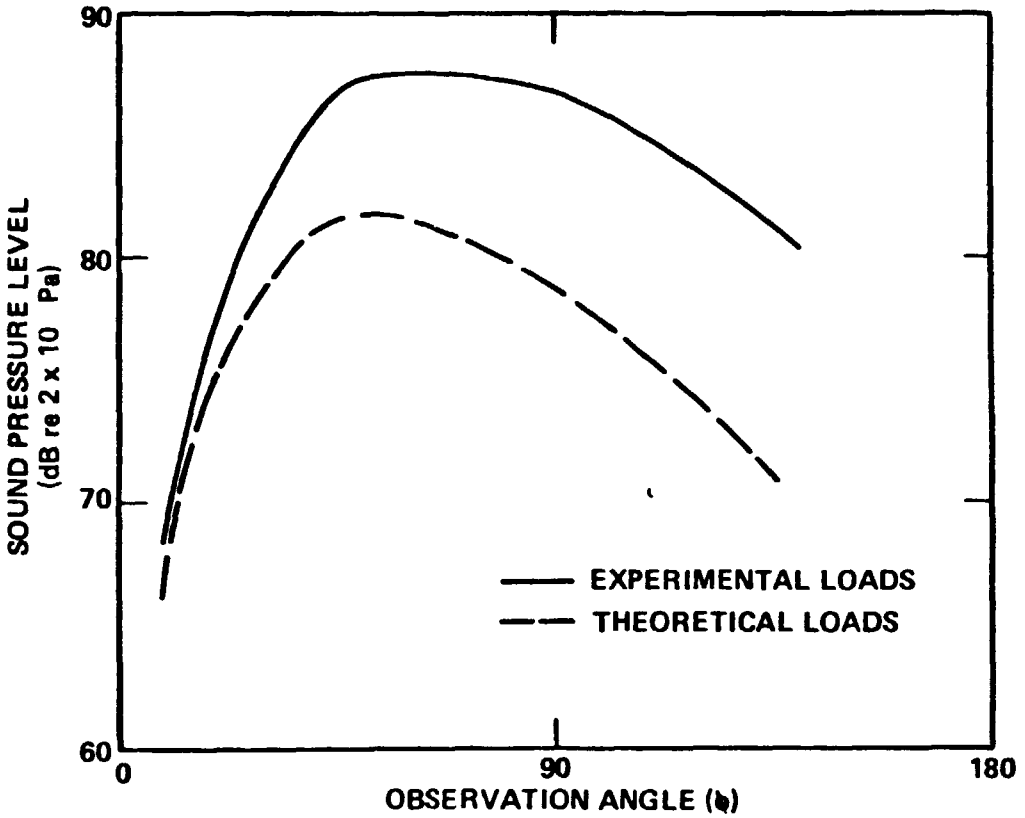

FIG. 6. CALCULATED FIRST HARMONIC OF THE LOADING NOISE (V = 41 M/SEC).

source of this disagreement is the incorrect calculation of the blade loads. Finally, as the helicopter recedes, the disagreement persists. As the helicopter recedes, the observer moves closer to the disk plane where the blade motion has a greater influence on the loading noise. However, the increasing influence of blade motion is not sufficient to overshadow the discrepancy in blade loading when the helicopter is receding.

To further explore the accuracy of noise predictions using theoretical load data a number of calculations were made. These calculations compare the calculated acoustic signature based on measured blade loads to the signature based on theoretical loads. Details of these computations may be found in Appendix A.

3.4 Narrowband Spectra

Figures 7 to 9 present the narrowband spectral analysis of the data. These analyses were computed at BBN from copies of the Bell acoustic data tapes. An analysis is performed at each of three speeds: 20, 41 and 67 m/sec, at a shallow observation angle. At 20 m/sec, the spectra at $\theta \approx 45°$ is also included as shown in Fig. 10.

On each plot, two angles are listed: ϕ gives the helicopter location when the signal is received; θ gives the helicopter location when the sound is emitted. The frequency domain of each spectra is from 0 to 200 Hz. The spectra are computed by centering a 2-sec interval about the appropriate point on the data tape and fast Fourier transforming the segment. This implies a bandwidth of 1/2 Hz, which yields approximately 20 frequency bins per blade passage period. This procedure is necessary to avoid overlap between adjacent harmonics. The procedure is quite adequate when the helicopter is moving slowly and close to the horizon. However, as the helicopter moves faster or approaches the overhead position, the procedure is less accurate. The reason is that the azimuthal location of the helicopter changes by a large amount in 2 sec under these conditions. In this study, the only place where helicopter motion in a 2-sec interval is especially large is at the $\theta \approx 90°$ overhead point.

Each of the predicted spectra in Figs. 7 to 9 uses the measured blade loads and includes an approximate correction for ground effect. Only comparisons using calculations on measured blade loads are presented. The calculations based on theoretical loads are inaccurate. Also, the measured data in

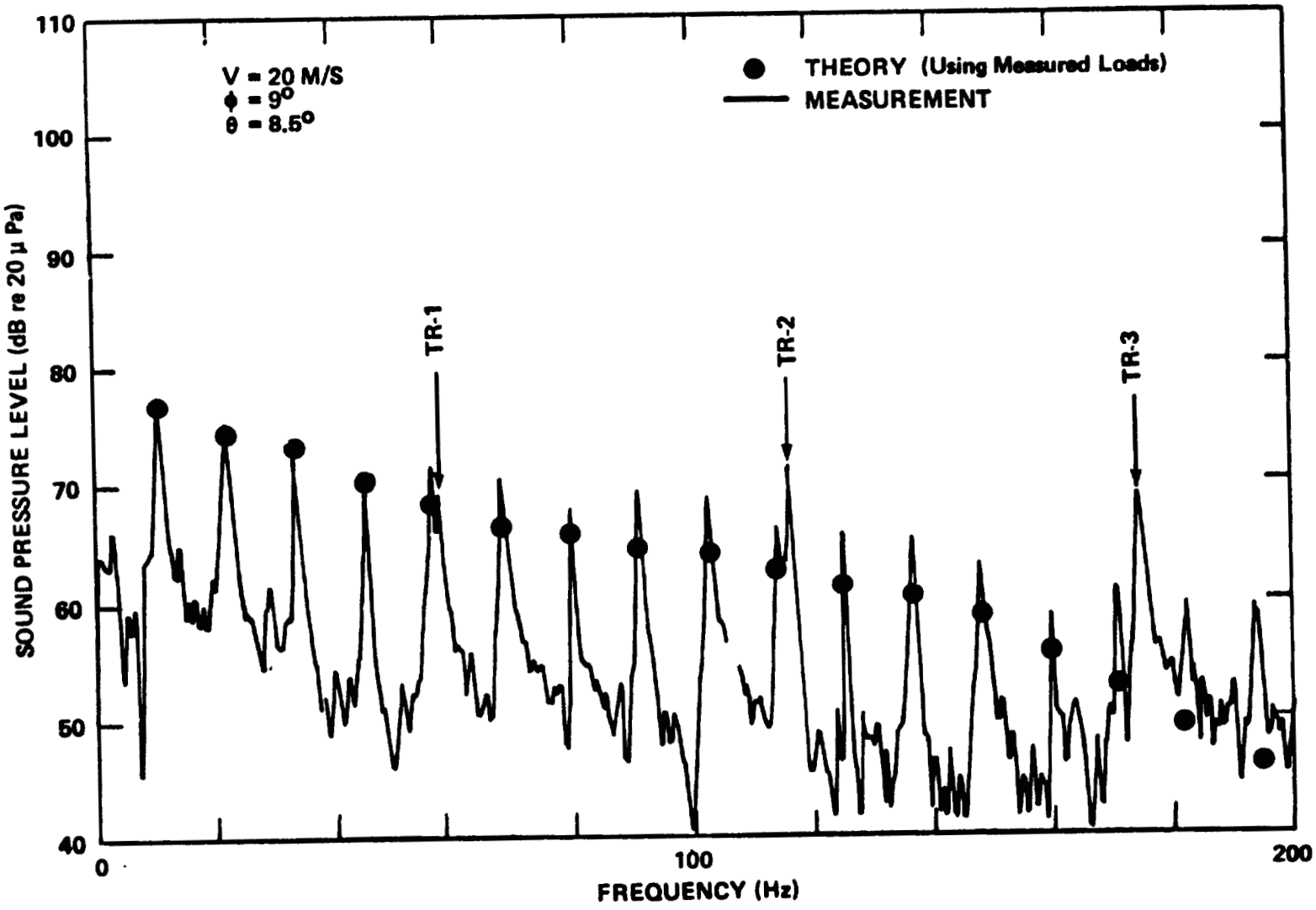

FIG. 7. THEORETICAL VS MEASURED NARROW BAND SPECTRA (V=20 M/S)

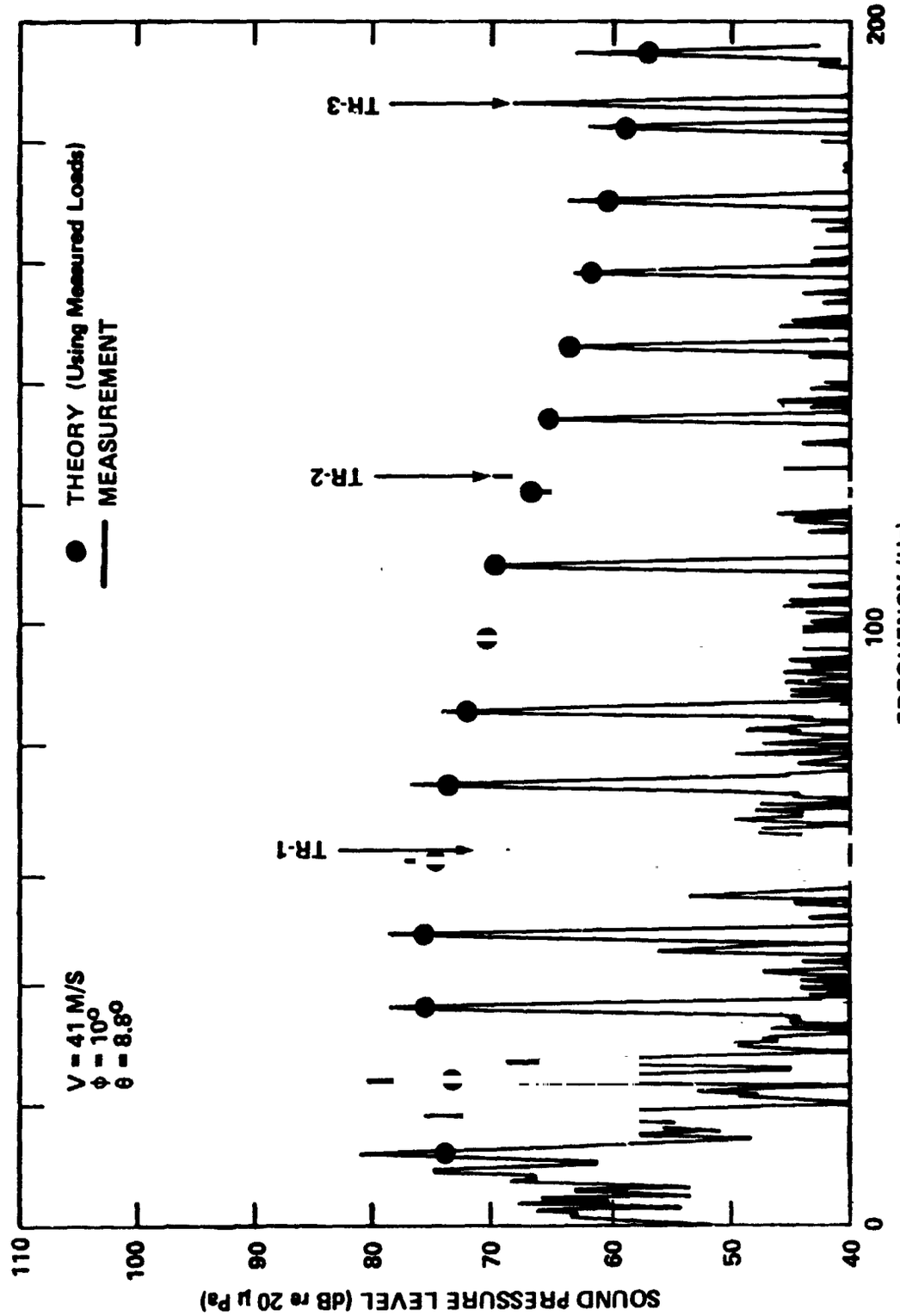

FIG. 8. THEORETICAL VS MEASURED NARROW BAND SPECTRA (V=41 M/S)

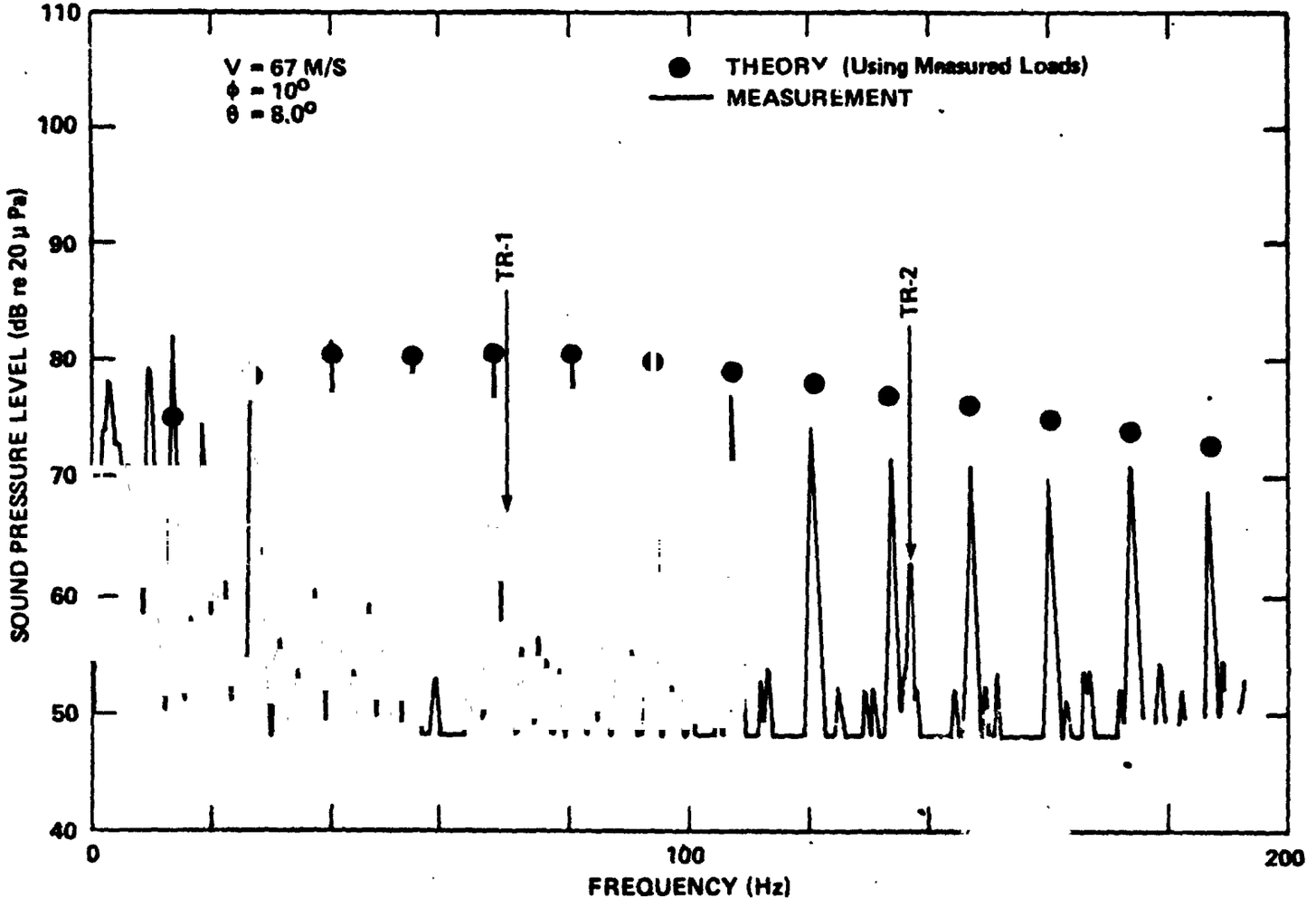

FIG. 9. THEORETICAL VS MEASURED NARROW BAND SPECTRA
(V=67 M/SEC)

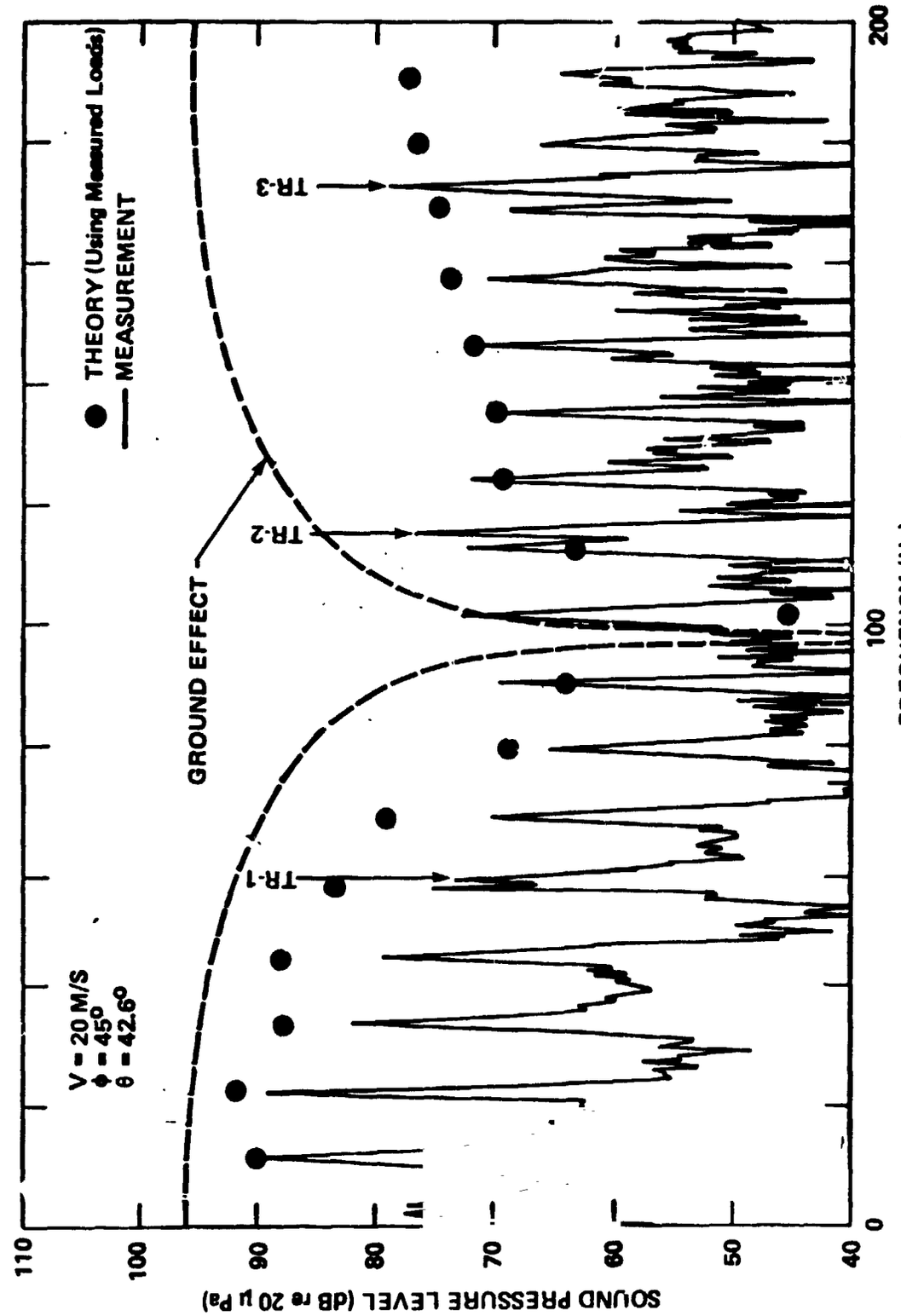

FIG.10 . EFFECT OF GROUND REFLECTION ON NARROW BAND SPECTRA (V=20 M/SEC)

Fig. 7 is adjusted for a suspected error. Details of this adjustment may be found in Appendix B. In all cases, the prediction and measurements show good agreement. At 41 and 67 m/sec, the agreement is possible because of the accurate calculation of blade thickness noise. Except for the low order harmonics blade loading is not important. At 20 m/sec, the agreement is due to an accurate model of the blade loads. Also note that the main rotor dominates the noise signature at all observation angles. This observation is important because later computations of the OASPL that ignore the contribution of the tail rotor will be made. These computations are justified only because the tail rotor noise level is less than that of the main rotor.

At the $\theta \approx 45°$ angle, the results change somewhat as shown in Fig. 10.

Theory and measurement agree at nearly all harmonics. However, an interesting discrepancy is found around the ninth harmonic ($f \approx 100$ Hz). Here, the level is grossly underpredicted. The reason is that the hard ground assumption implies almost complete destructive interference near this frequency. It is clear that such an effect is not observed.

Recall that the ground reflection coefficient is assumed equal to 1. For reflection coefficients equal to 1, the Fourier spectra are modulated by the following term

$$10 \log \left[2 \cos\left(\frac{\omega}{c} h \sin\theta\right)\right]^2 . \qquad (4)$$

Here ω is the angular frequency, c is the sound speed, h is the microphone height, and θ is the angle at which the sound is emitted. Note the complete destructive interference occurs when the cosine function equals zero, which corresponds to a frequency of 98 Hz in Fig. 10. Complete destructive interference is never observed experimentally because of the random phase shifts between the direct and reflected signal, which are caused by fluctuations in the atmosphere, and also because the reflection coefficient is not exactly 1.

Additional comparisons between measured and predicted narrowband spectra are presented in Appendix B. Comparisons of measured spectra are made to calculated spectra based on

both measured and theoretical blade loads. Also, the problems associated with computing spectra from a moving helicopter are reviewed in greater detail.

3.5 Flyover Noise Levels

Figures 11 to 13 give the calculated noise level versus observation angle at three vehicle speeds: 20, 41, and 67 m/sec. These speeds represent the lowest, middle, and highest speeds available from the OLS database.[2] The measured OASPL are computed from the acoustic data tapes containing the pressure time histories. The data tapes are divided into 1/2-sec increments, and then each data sample is reduced to OASPL. The acoustic calculations are based on the measured blade loads. The calculations are adjusted for the influence of the ground. All calculations are plotted as a function of the angular location of the helicopter.

One interesting feature is the shape of the curves. The low-speed noise curve is approximately symmetric and reaches its maximum when the helicopter is overhead, $\theta \approx 90°$. The high-speed noise curve, however, is asymmetric with the peak shifted to an earlier time when the helicopter is approaching the observer, $\theta \approx 30°$. This trend is also evident in the calculated values.

The calculation shows that the asymmetry is due to the increasing influence of the "thickness" noise contribution with increasing helicopter speed. The thickness noise is greatest when the helicopter approaches the observer. As the helicopter passes overhead, the thickness noise is minimal and does not increase until the helicopter is receding toward the opposite horizon. (See Figs. 14 to 16.)

The asymmetry in the thickness noise is due to the variation in the speed at which the blade approaches the observer. This asymmetry does not appear in the calculated loading noise. The reason is that noise due to unsteady force dominates the loading noise when the vehicle is overhead. This unsteady noise is due to the term $\partial L_i/\partial t$ in Eq. (1). If the loading did not depend on time, the loading noise would have the same asymmetrical dependence on observation angle as the thickness noise.

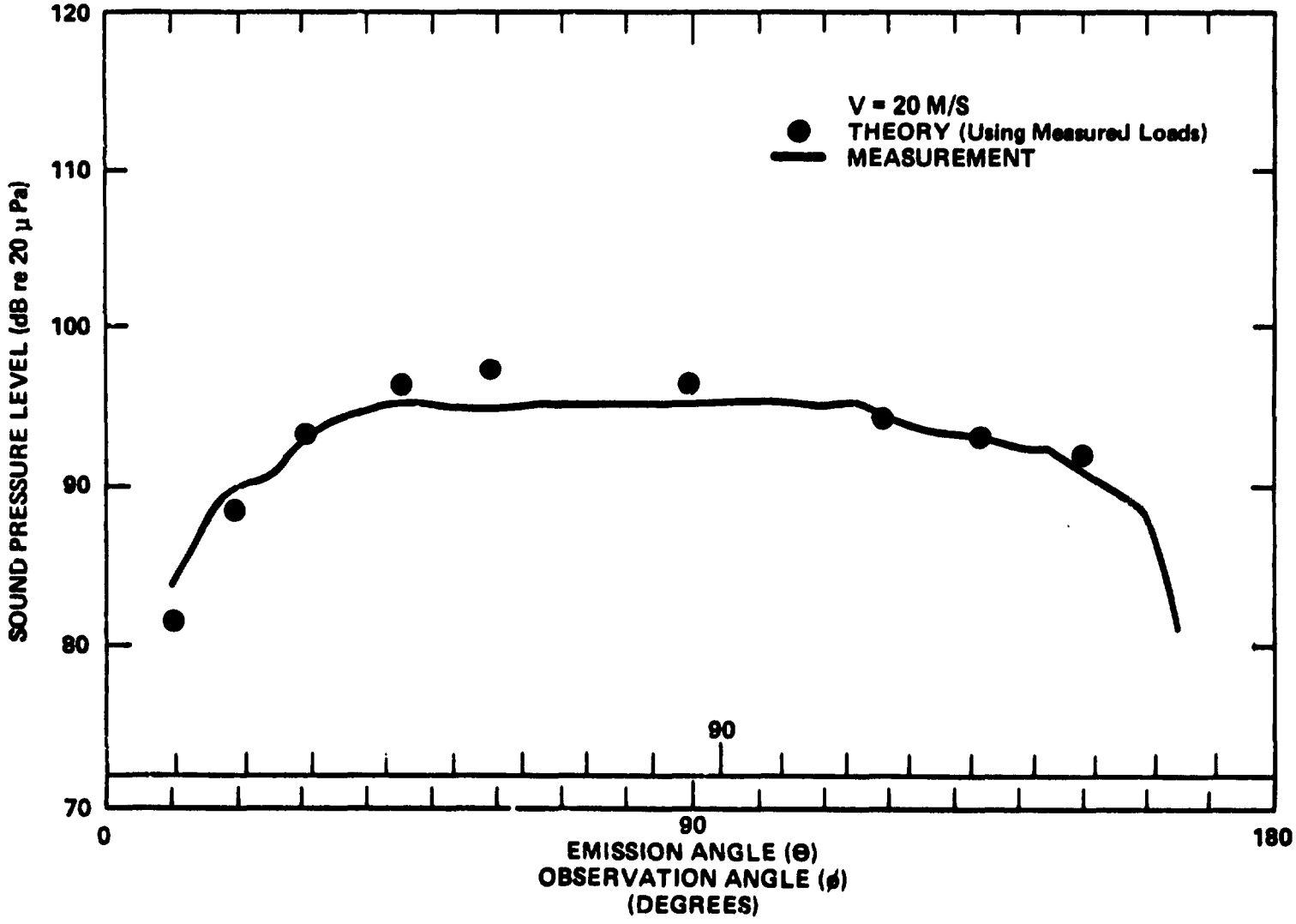

FIG. 11 THEORETICAL MEASURED OASPL
(V=20 M/SEC)

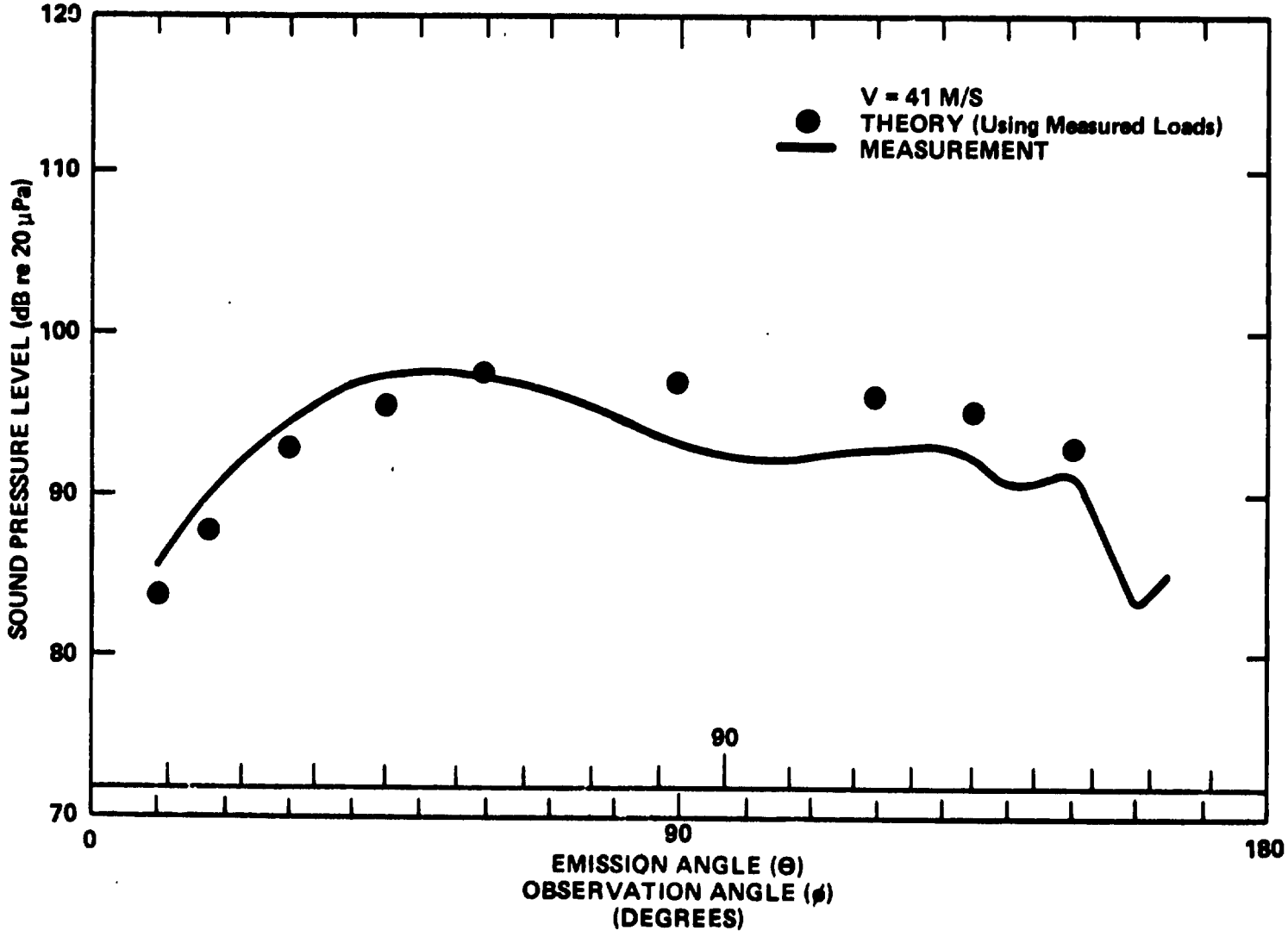

FIG. 12. THEORETICAL VS MEASURED OASPL

(V=41 M/SEC)

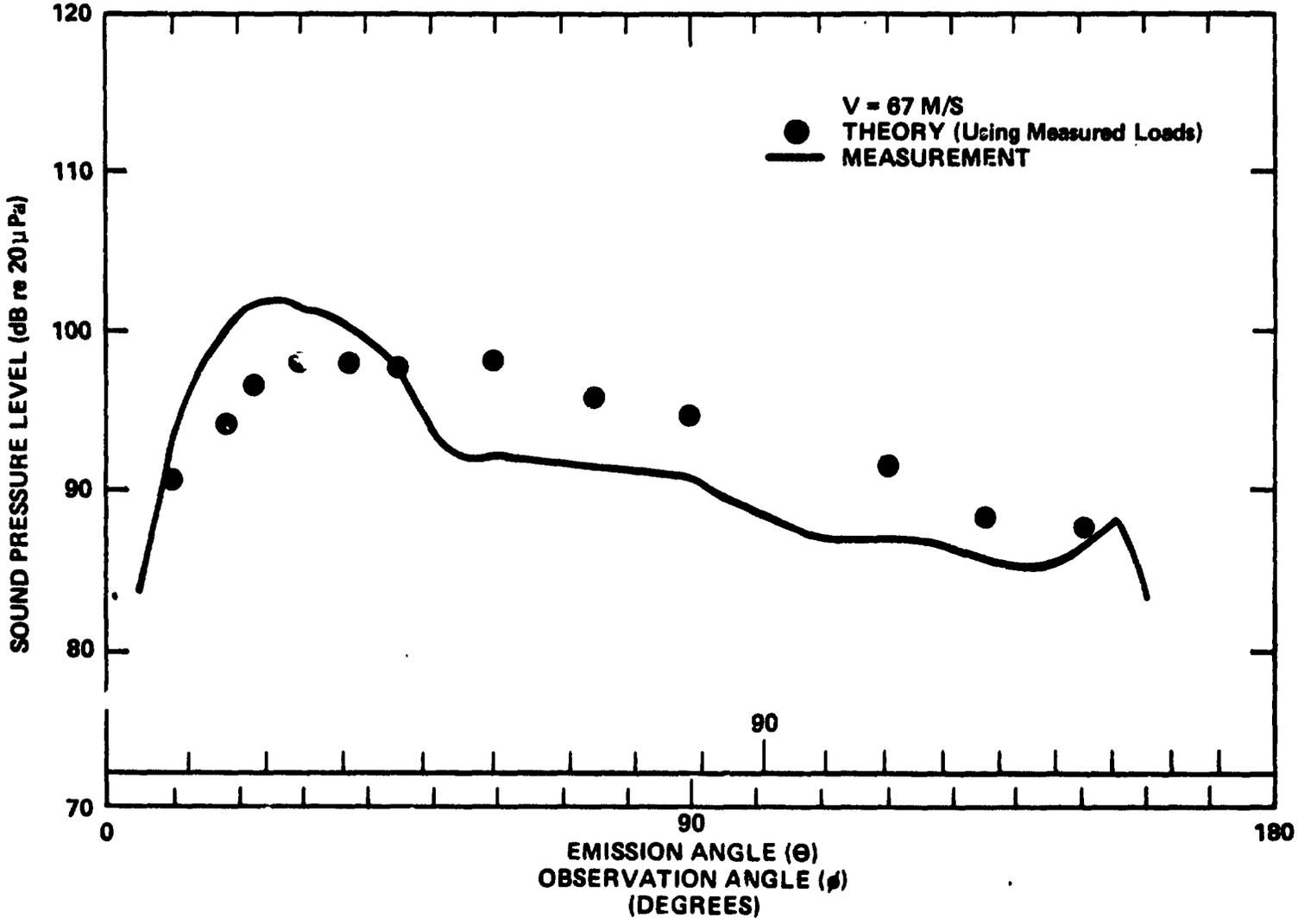

FIG. 13. THEORETICAL VS MEASURED OASPL
(V=67 M/SEC)

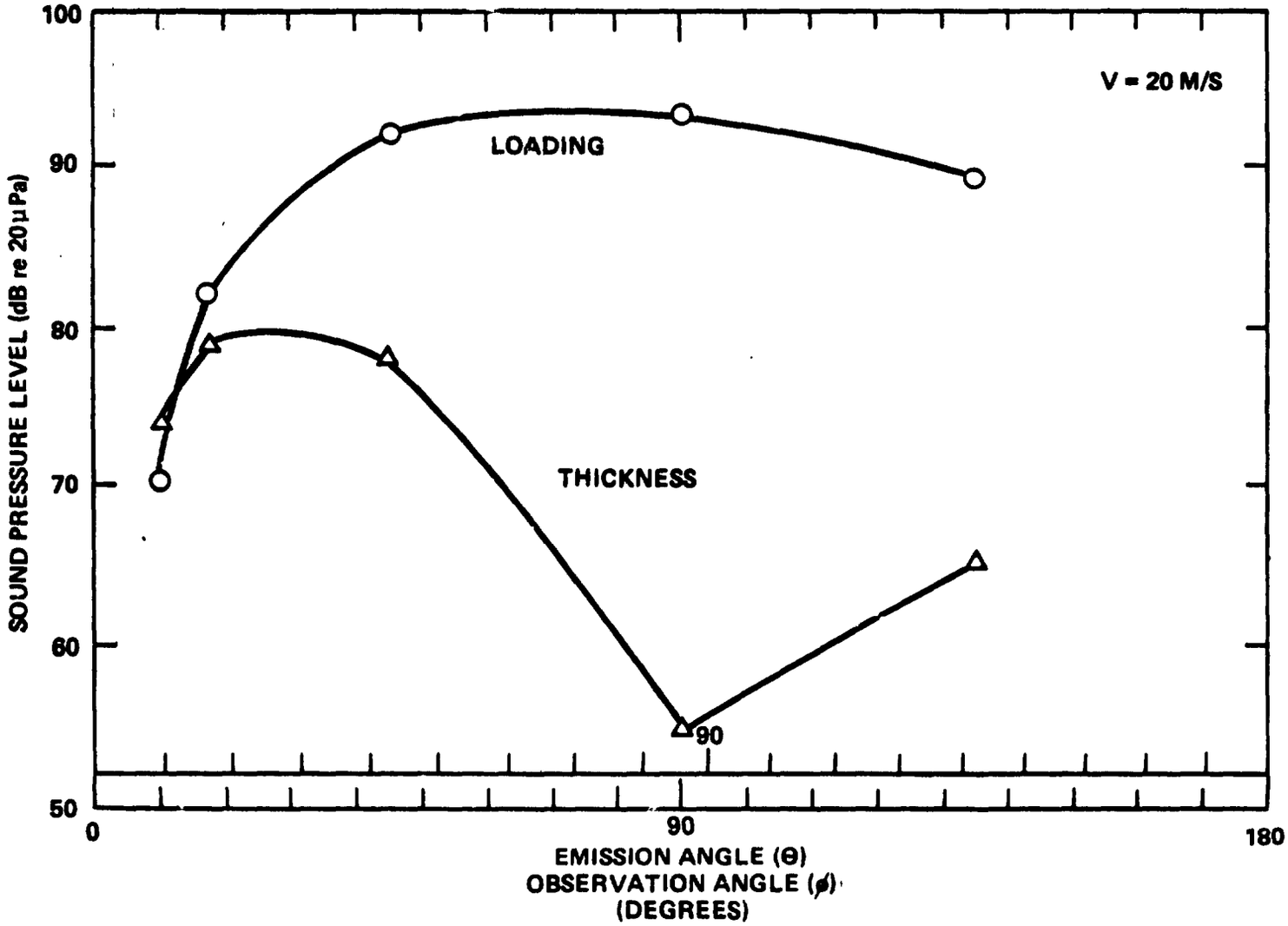

FIG. 14. RELATIVE INFLUENCE OF THICKNESS AND LOADING NOISE (V= 20 M/SEC)

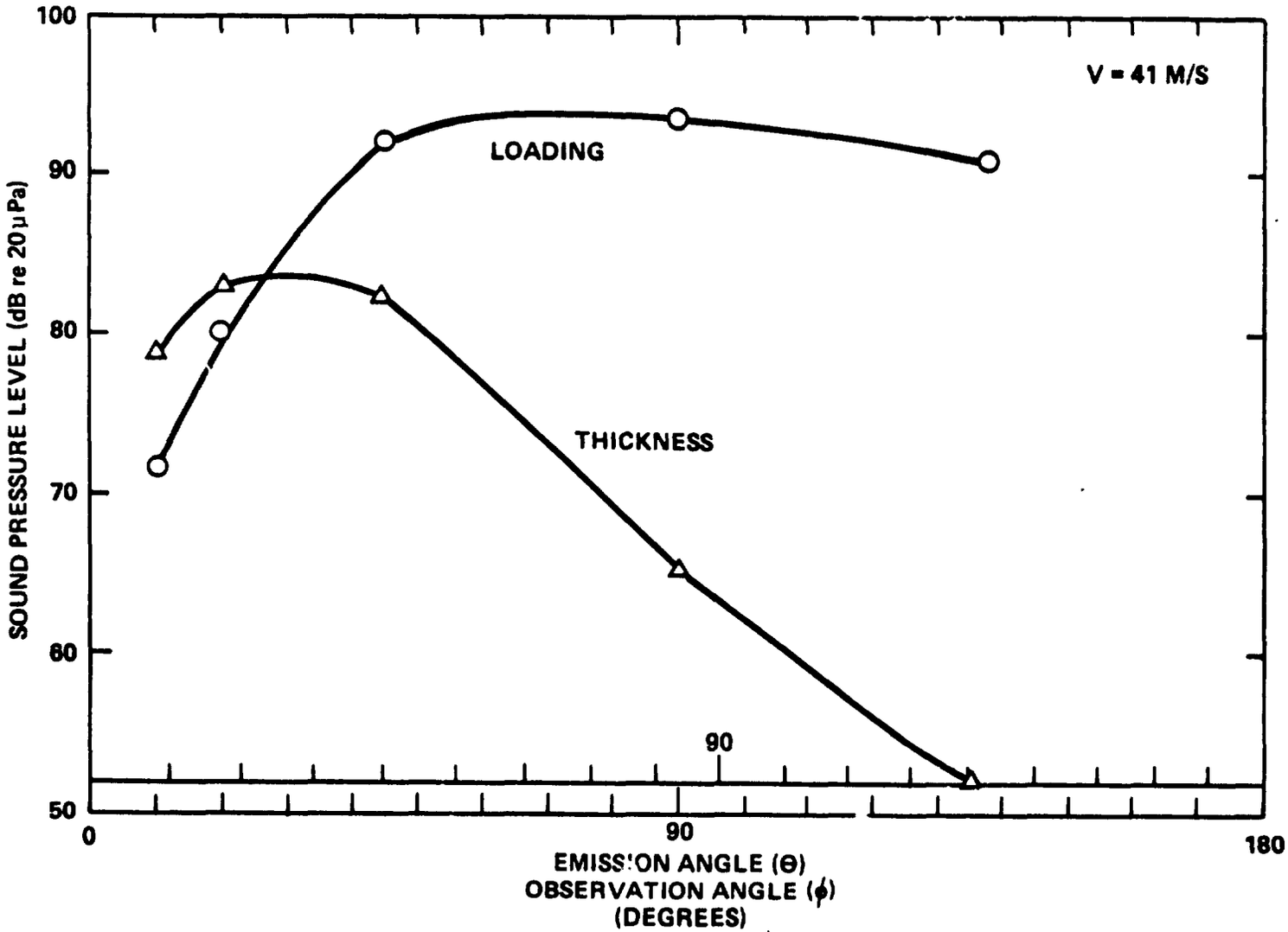

FIG. 15. RELATIVE INFLUENCE OF THICKNESS AND LOADING NOISE (V=41 M/SEC)

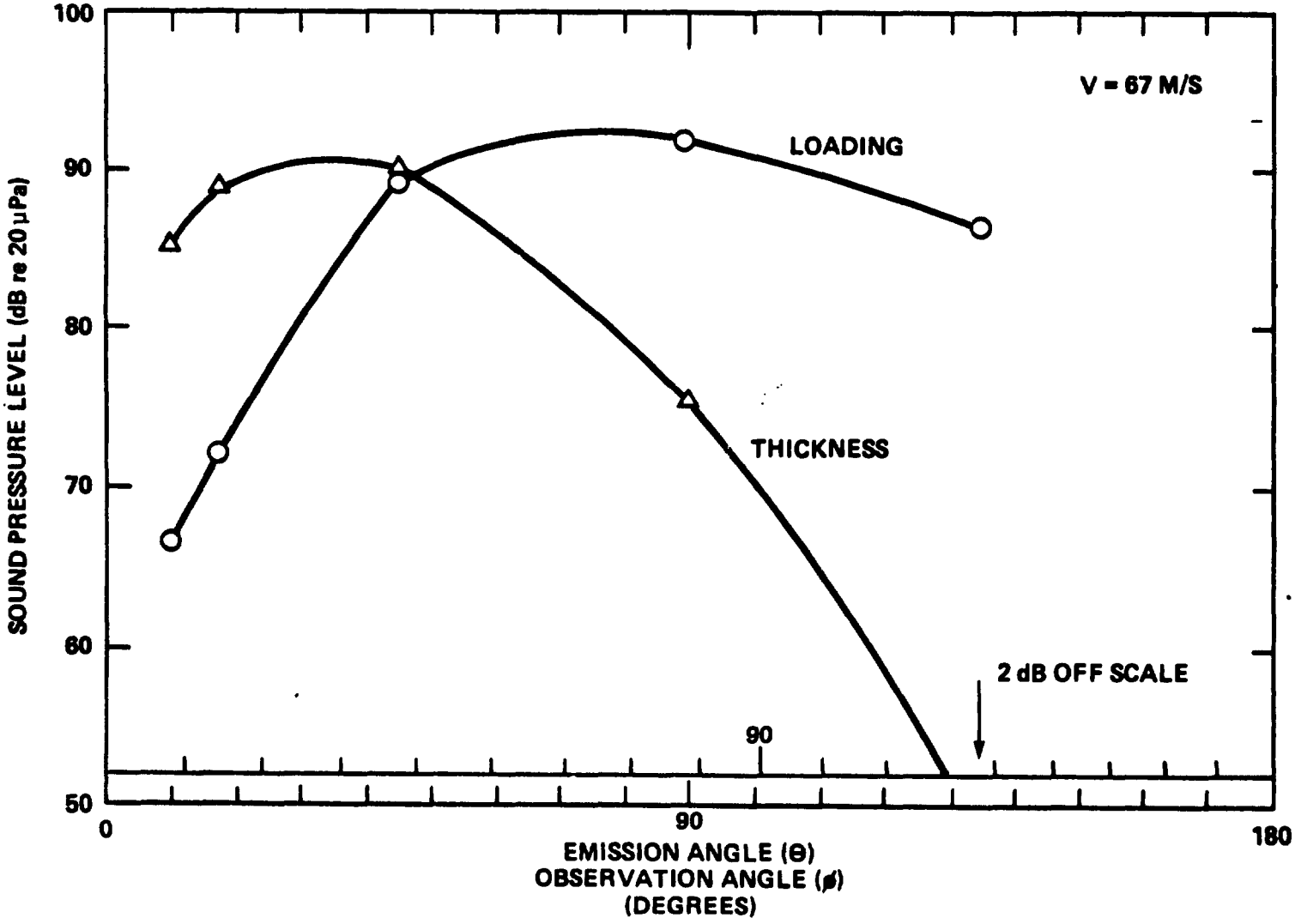

FIG. 16. RELATIVE INFLUENCE OF THICKNESS AND LOADING NOISE (V=67 M/SEC)

Finally, as shown in Figs. 11 to 13, the noise prediction is best at low speeds and worst at high speeds. At high speeds (Fig. 13), the calculated noise is smaller than the measured noise. The discrepancy is greatest when the observer is near the disk plane. This observation suggests a possibility for improving the agreement. One could include the forces parallel to the chord. Near the disk plane, the ray from source to observer is approximately parallel to the blade chord. Forces parallel to the chord are not considered in this paper. Including these forces will increase the magnitude of the term $\hat{r}_i \cdot L_i$ in Eq. (2) and thereby increase the calculated noise.

4. CONCLUSIONS

Accurate agreement between theoretical and measured helicopter rotational noise is possible if the measured blade loads are used in the computations. In particular, accurate agreement is found when the helicopter is overhead. Overhead, the helicopter is at a particularly difficult location for noise prediction because the noise field is determined primarily by the unsteady loads. Accurate agreement here is possible only because of the accurate blade load input.

Some discrepancy between the measured and predicted noise is found at the highest helicopter velocity investigated (67 m/sec). At this speed, the noise is underpredicted when helicopter is approaching the observer. A possibility for improving the prediction is to consider the influence of forces parallel to the blade chord. The influence of these forces is to increase the predicted noise and thereby bring the predictions into better agreement with theory.

An evaluation of helicopter noise predictions using theoretical loads as the basis for the calculation is also made. Accurate predictions based on theoretical loads are only possible for a narrow set of observer locations. At these observer locations, the predicted noise field is dominated by the influence of blade motion. When the helicopter is overhead, accurate predictions based on theoretical blade loads are not possible. To make better predictions, it is necessary to model the blade loads more accurately than is possible with the scheme used herein.

REFERENCES

1. "Noise Standards for Helicopters in the Normal, Transport, and Restricted Categories," FAA NPRM 79-13, Federal Register, Vol. 44, No. 140, 19 July 1979.

2. Proposed Amendment 5, International Standards and Recommended Practices, "Aircraft Noise," Annex 16 to the Convention on International Civil Aviation, 1980, ICAO, Quebec, Canada.

3. Succi, G.P. and Brieger, J.T., "Prediction of Helicopter Rotor Noise from Measured Blade Surface Pressure," American Helicopter Society, 37 Annual Forum Proc., May 1981.

4. Nystrom, P. A., and Farassat, F., "A Numerical Technique for Calculation of the Noise of High Speed Propellers with Advanced Blade Geometry," NASA TP 1662, 1980.

5. Davis, S, Jon, and Egolf, T. Alan, "An Evaluation of a Computer Code Based on Linear Acoustic Theory for Predicting Helicopter Main Rotor Noise," NASA Contractor Report 159339, July 1980.

6. Shockey, G. A., Williamson, J. W., and Cox, C. R., "AH-1G Helicopter Aerodynamic and Structural Loads Survey," USAAMRDL-TR-76-39, Bell Helicopter Textron, February 1977.

7. Cox, C. R., "Helicopter Rotor Aerodynamic and Aeroacoustic Environments," 4th Aeroacoustics Conference, American Institute of Aeronautics and Astronautics, October 1977.

8. Brieger, J. T., "Validation of Helicopter Noise Prediction Techniques - Data Base," Bell Helicopter Textron, Report No. 699-099-119, January 1980.

9. Farassat, F., and Succi, G. P., "A Review of Propeller Noise Prediction Technology with Emphasis on Two Current Methods for Time Domain Calculations," J. Sound Vib., 71, 399-419, August 1980.

10. Scully, M. P., "Computation of Helicopter Rotor Wake Geometry and Its Influence on Rotor Harmonic Airloads," ASRL TR 178-1, March 1975.

11. Embleton, T. F. W., et al., "Outdoor Sound Propagation Over Ground of Finite Impedance," J. Acoust. Soc. Amer. 59, 267-77, February 1976.

12. Succi, G. P., "Design of Quiet Effective Propellers," Society of Automotive Engineers Paper 790584, April 1979.

13. Gutin, L., "On the Sound Field of a Rotating Airscrew," 1936 Zhurnal Technicheskoi Fiziki 6, 8999-909. (in Russian) (Translated as 1948 NACA TM-195.)

14. Lowson, M. V., "The Sound Field for Singularities in Motion," Proceedings of the Royal Society (London), A286, 559-572, 1965.

APPENDIX A: COMPARISONS OF CALCULATED PRESSURE TIME SIGNATURES BASED ON MEASURED AND THEORETICAL BLADE LOADS

A set of computations was made to evaluate the accuracy of acoustic signatures based on theoretical blade loads. These computations compare the acoustic signature based on theoretical loads to the signature based on measured loads. All the measured blade loads are from a single rotation period. This procedure is used to accurately represent the maximum pressure that can occur due to sudden change in the blade loads. All the theoretical loads are from Scully's model[10] of the blade response to a rigid skewed helical vortex sheet. A more elaborate model is available, however, it is not much more accurate than the model of rigid wake airloads.

Here the acoustic signatures for the "combined loading noise" are presented. This is the loading noise which includes both near and far field terms. Both helicopter position and speed are considered. The test cases are detailed in Table A1. These data are later used to compute noise spectra for comparison to the measured spectra in Appendix B. Each position ϕ corresponds to a measured helicopter location as deduced from the time code on the tape.

The figures are organized by the observation angle (ϕ). For each observation angle data for 20, 41, and 67 m/sec is presented. The loading noise is similar only when the helicopter is approaching an observer who is approximately in the disk plane ($\phi \approx 10°$, Figs. A1 to A3). At this observation angle blade motion effects are more important than details of the blade loads. For observations made at a slightly greater angle to the disk plane the two calculations begin to disagree ($\phi \approx 17°$, Figs. A4 to A6). This discrepancy increases at larger observation angles ($\phi \approx 45°$, Figs. A7 to A9), and is most pronounced when the helicopter is overhead ($\phi \approx 90°$, Figs. A10 to A12) and persists as the helicopter recedes from the observer ($\phi \approx 140°$, Figs. A13 to A15). Thus, whenever the details of the blade loading are more important than blade motion, calculations based on theoretical loads are inaccurate.

TABLE A1.

V (m/sec)	20		41		67	
Approximate Observation Angle ϕ	θ	Fig.	θ	Fig.	θ	Fig.
10°	8.46	A1	8.80	A2	8.05	A3
17°	17.65	A4	15.05	A5	13.36	A6
45°	42.49	A7	40.06	A8	36.99	A9
90°	86.46	A10	83.07	A11	78.63	A12
140°	137.51	A13	139.85	A14	143.01	A15

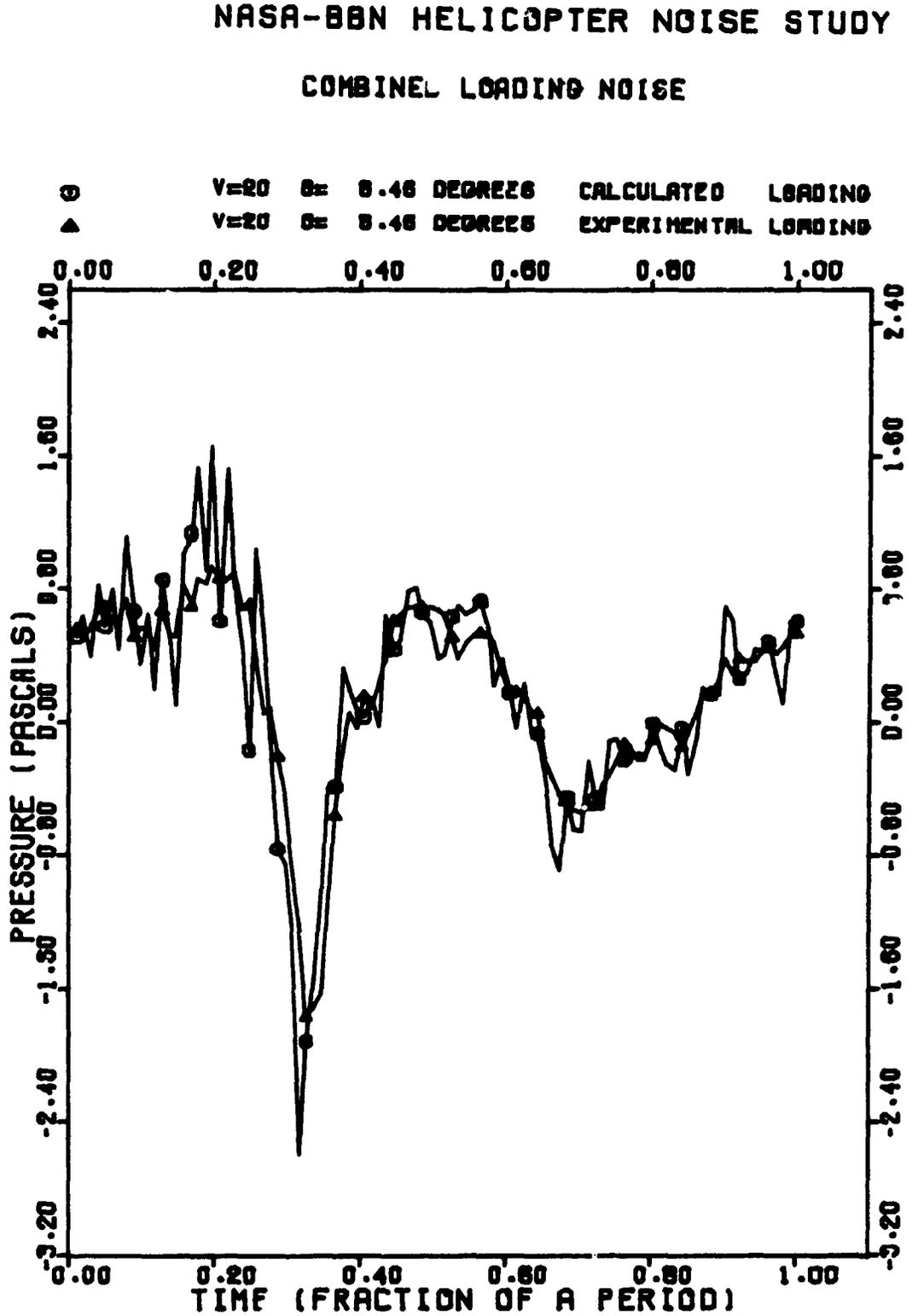

FIG. A1. COMBINED LOADING NOISE CALCULATED FROM MEASURED AND THEORETICAL BLADE LOADS V = 20 m/sec, θ = 8.46°, $\phi \approx 10°$.

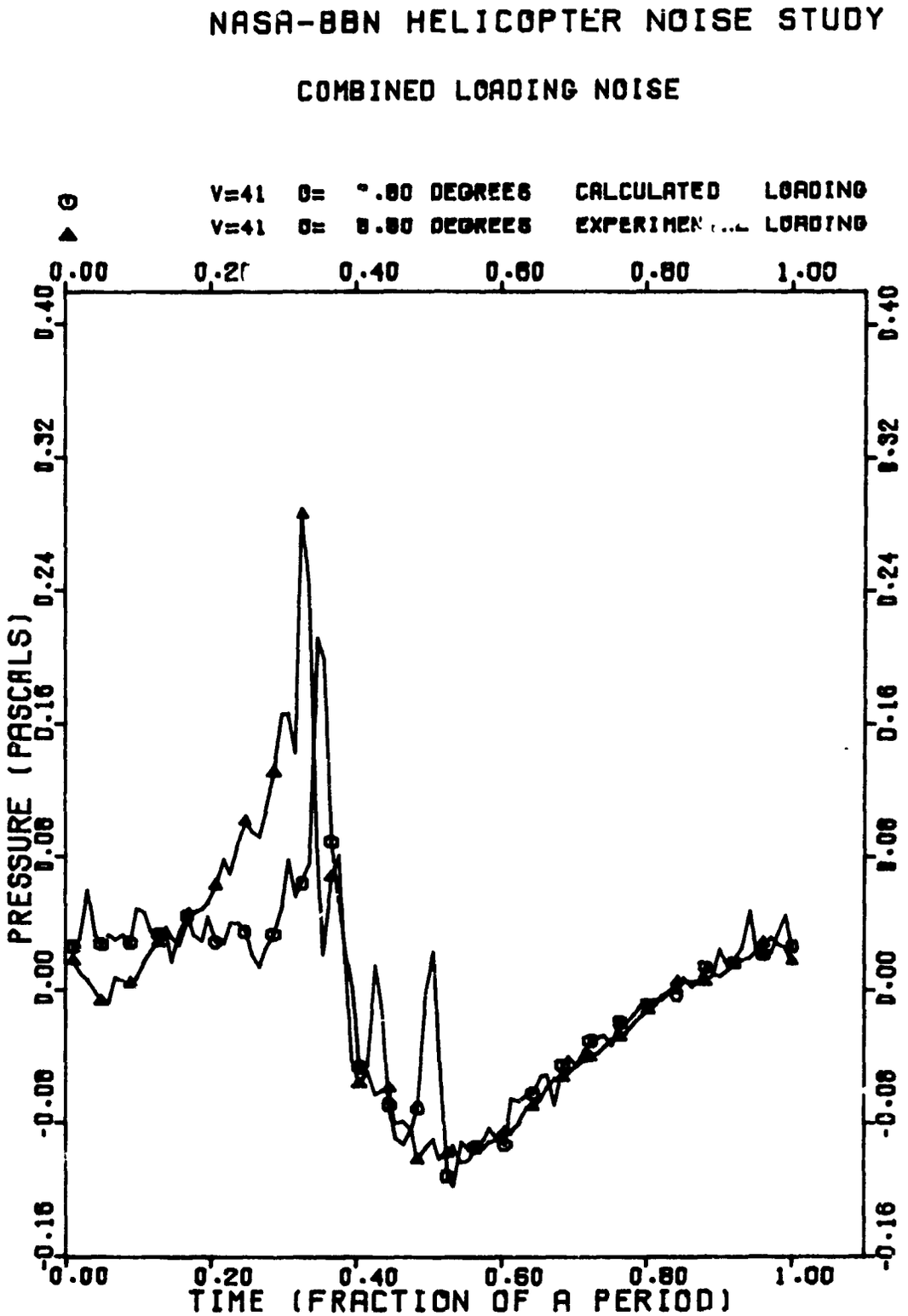

FIG. A2. COMBINED LOADING NOISE CALCULATED FROM MEASURED AND THEORETICAL BLADE LOADS V = 41 m/sec, $\theta = 8.80°$, $\phi \approx 10°$.

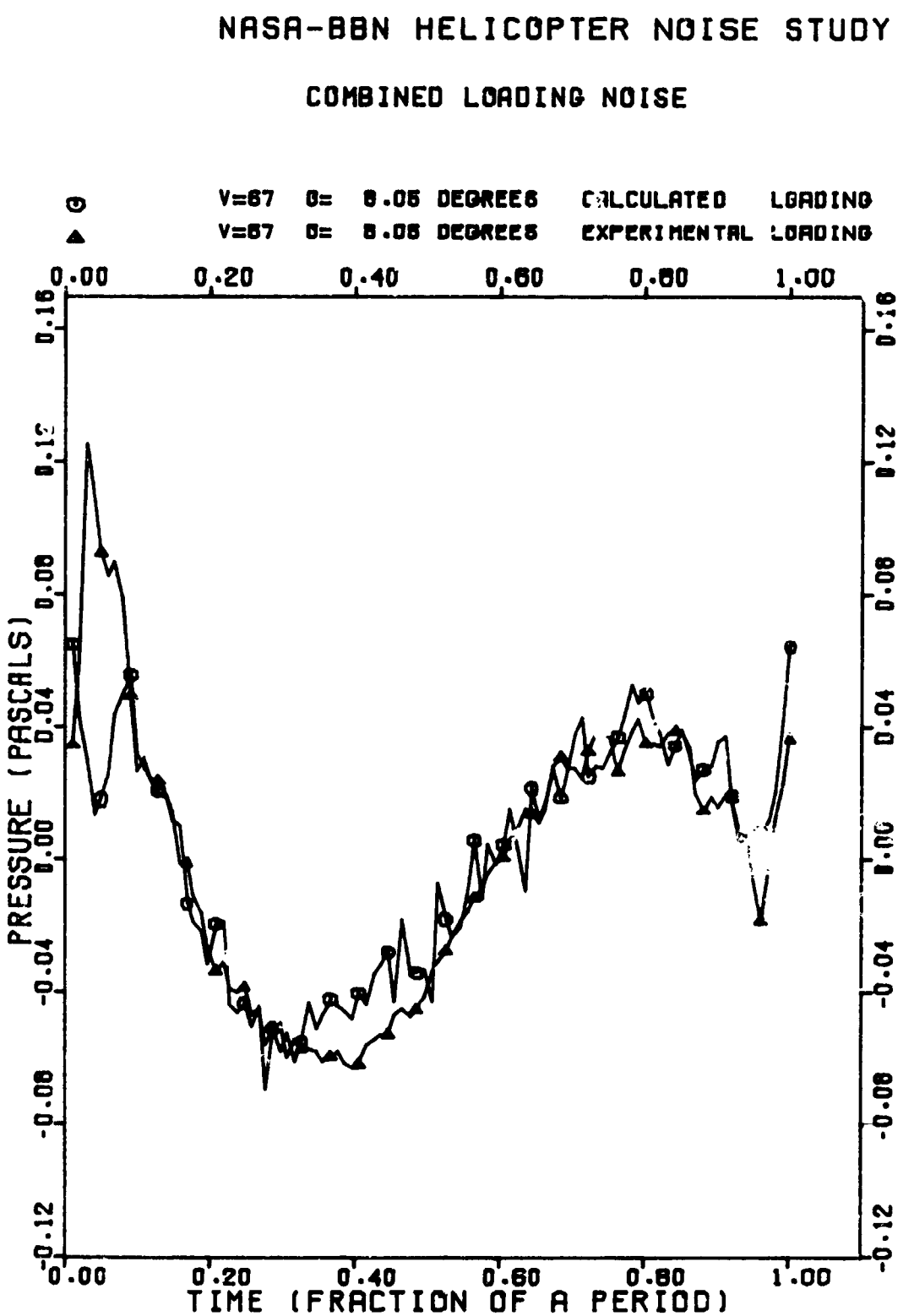

FIG. A3. COMBINED LOADING NOISE CALCULATED FROM MEASURED AND THEORETICAL BLADE LOADS V = 67 m/sec, θ = 8.05°, $\phi \approx 10°$.

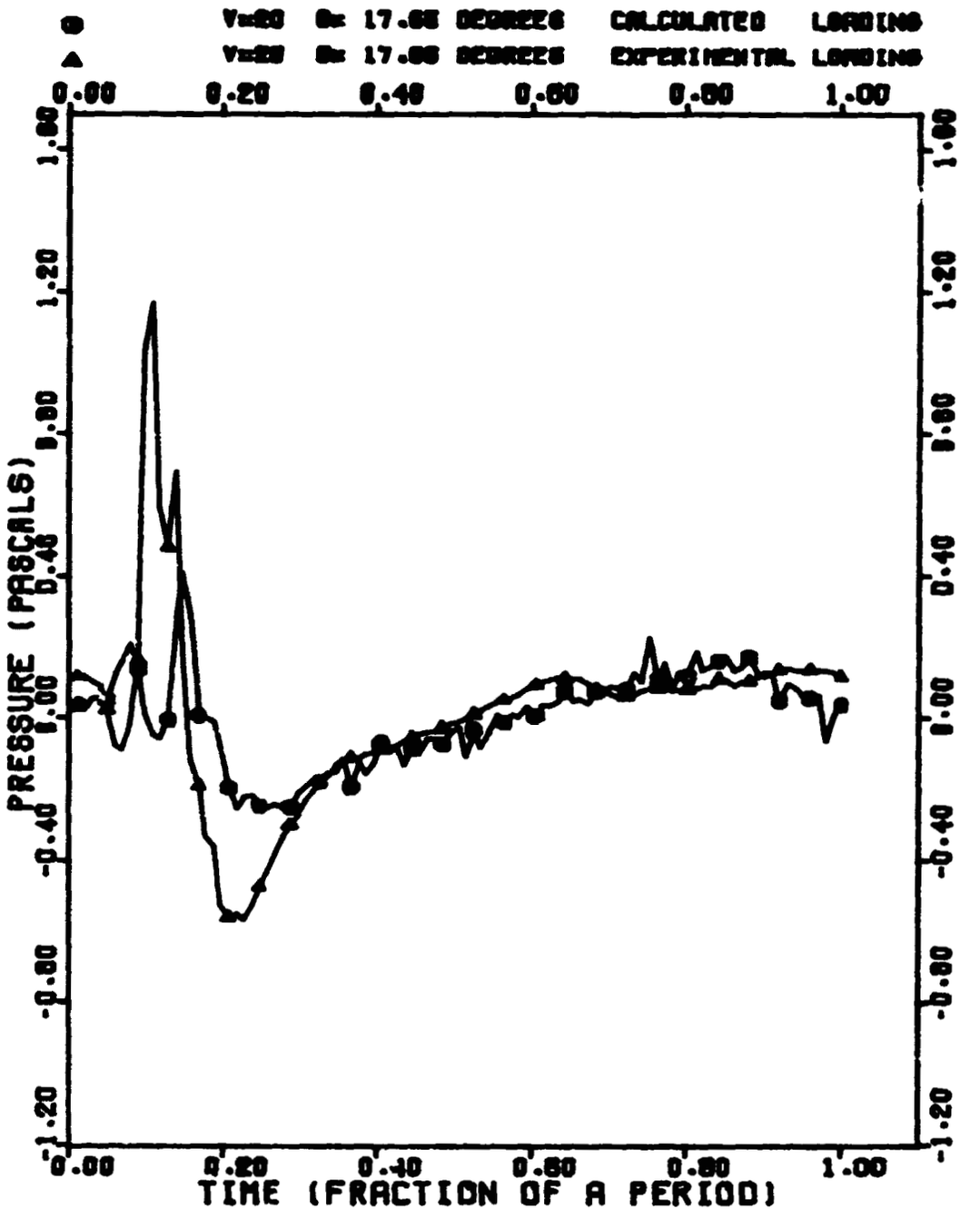

FIG. A4. COMBINED LOADING NOISE CALCULATED FROM MEASURED AND THEORETICAL BLADE LOADS V = 20 m/sec, θ = 17.65°, $\phi \approx 17°$.

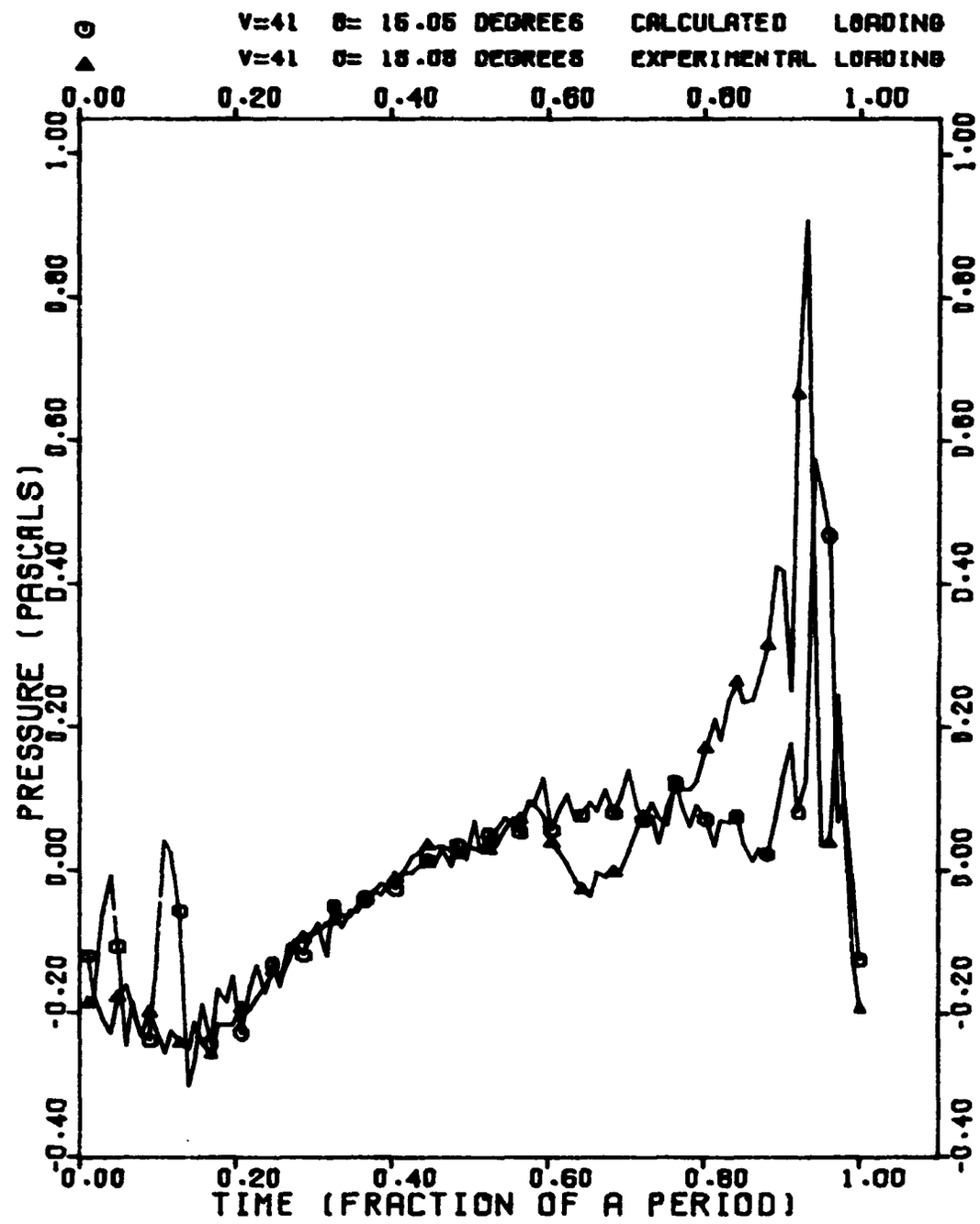

FIG. A5. COMBINED LOADING NOISE CALCULATED FROM MEASURED AND THEORETICAL BLADE LOADS V = 41 m/sec, θ = 15.05°, $\phi \simeq 17°$.

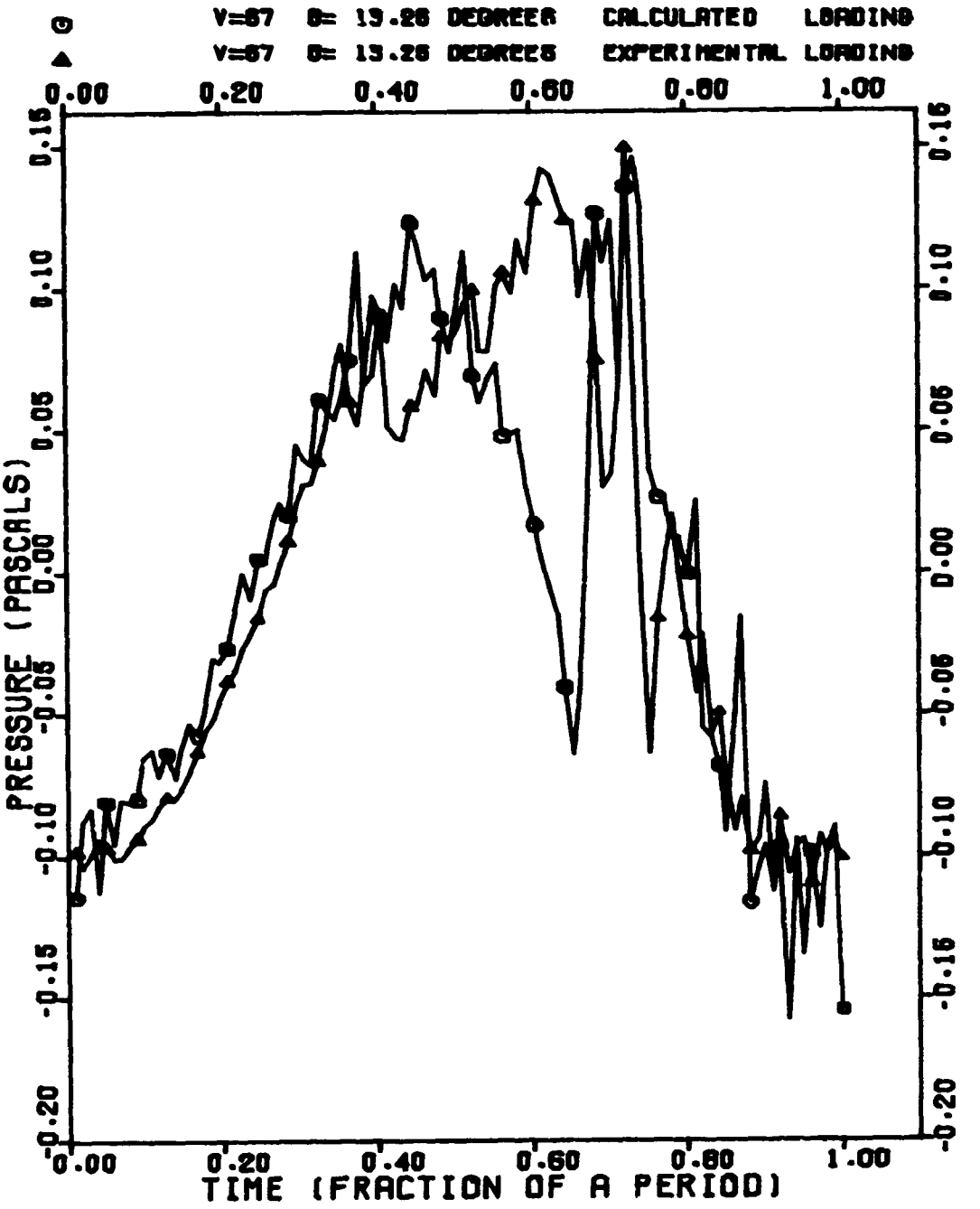

FIG. A6. COMBINED LOADING NOISE CALCULATED FROM MEASURED AND THEORETICAL BLADE LOADS V = 67 m/sec, θ = 13.26°, $\phi \approx 17°$.

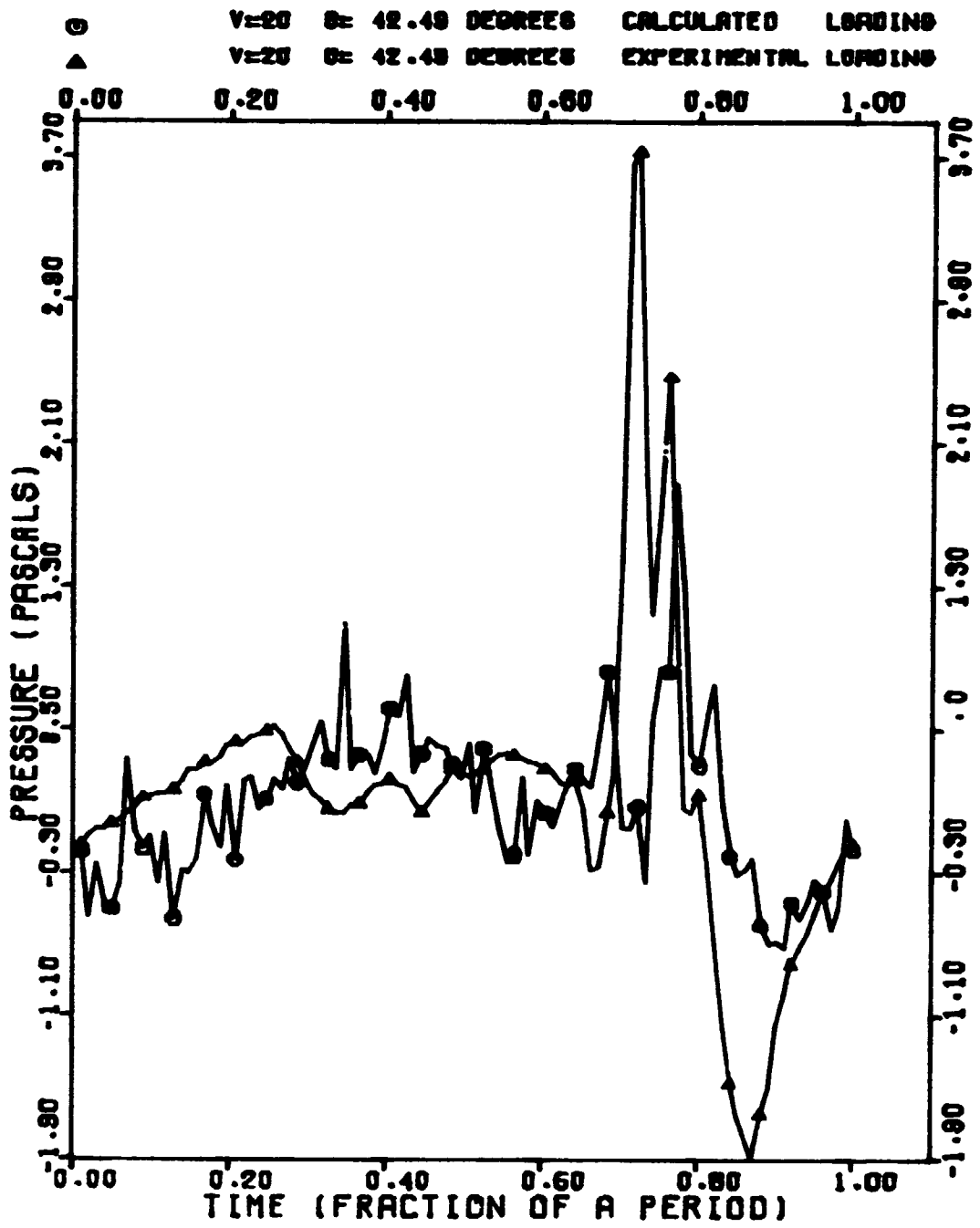

FIG. A7. COMBINED LOADING NOISE CALCULATED FROM MEASURED AND THEORETICAL BLADE LOADS V = 20 m/sec, $\theta = 42.49°$, $\phi \approx 45°$.

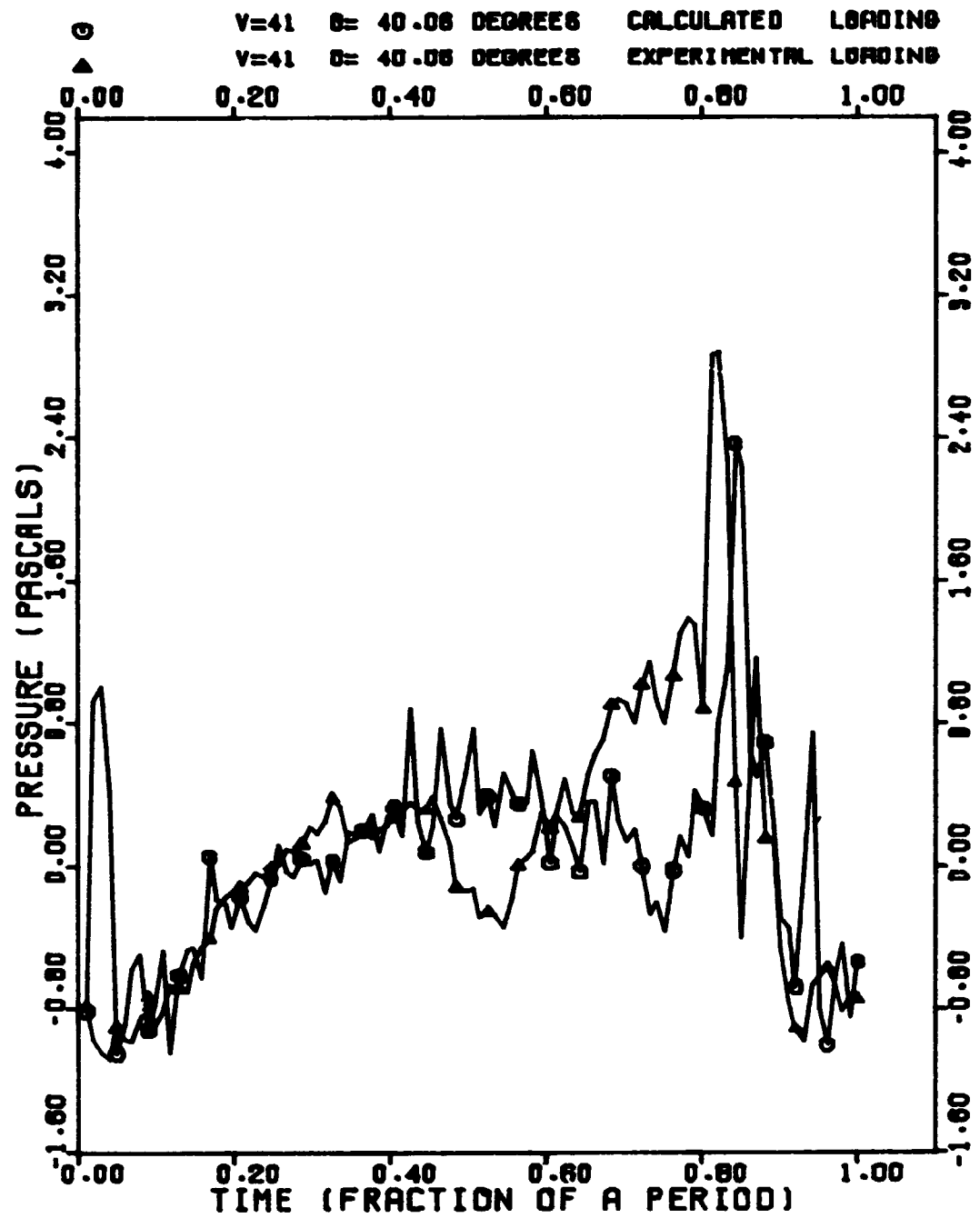

FIG. A8. COMBINED LOADING NOISE CALCULATED FROM MEASURED AND THEORETICAL BLADE LOADS V = 41 m/sec, θ = 40.06°, $\phi \approx 45°$.

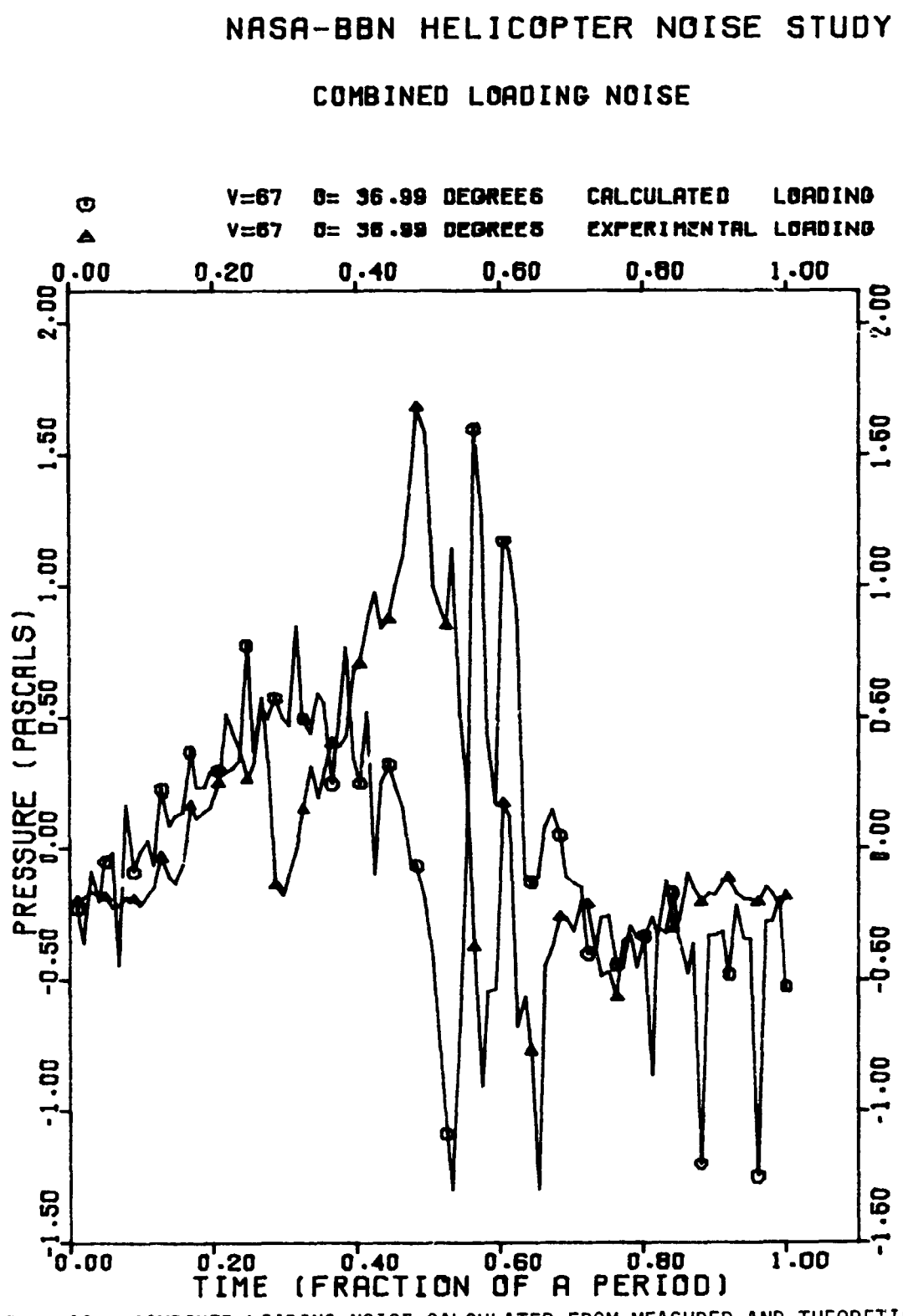

FIG. A9. COMBINED LOADING NOISE CALCULATED FROM MEASURED AND THEORETICAL BLADE LOADS V = 67 m/sec, θ = 36.99°, $\phi \approx 45°$.

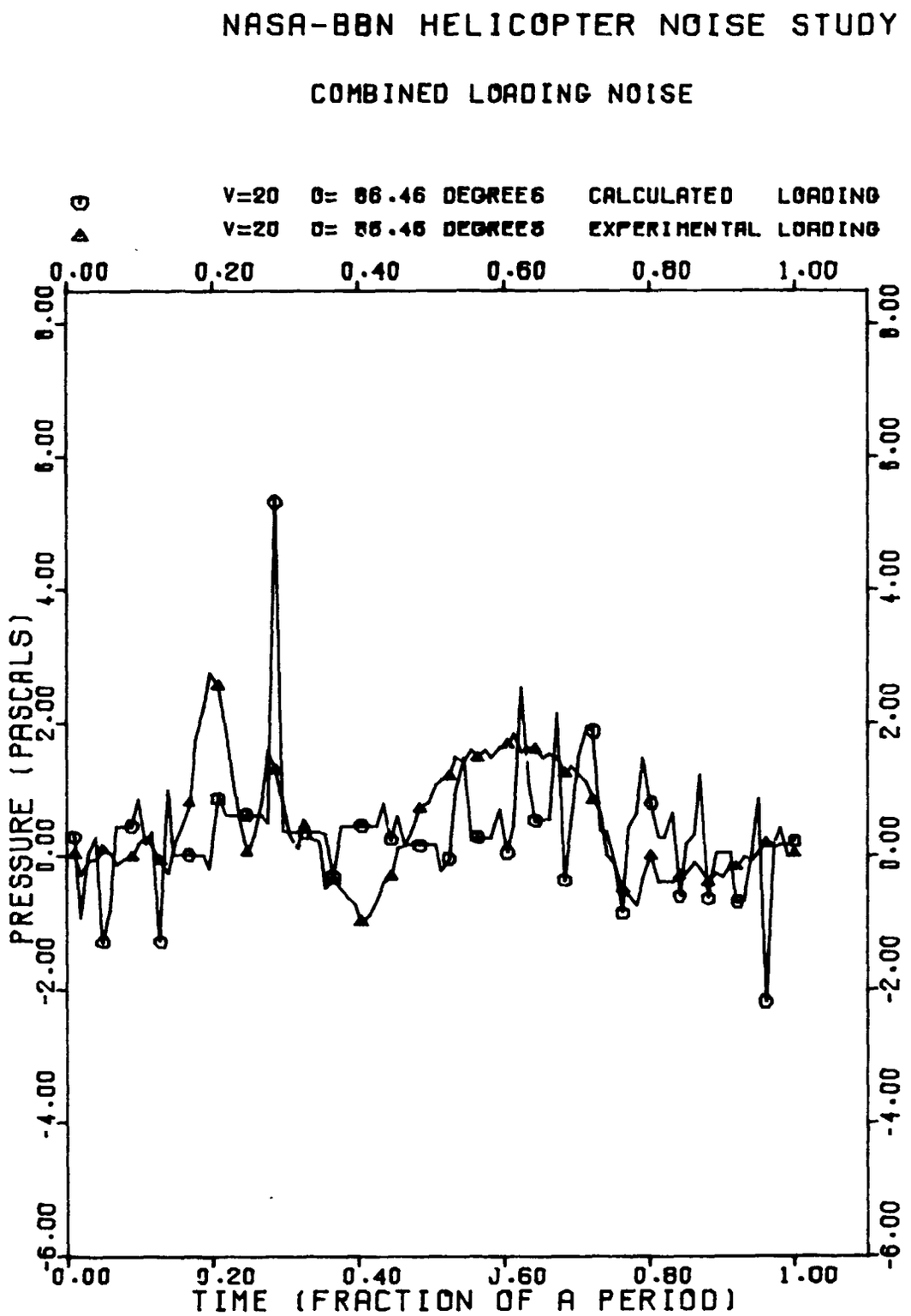

FIG. A10. COMBINED LOADING NOISE CALCULATED FROM MEASURED AND THEORETICAL BLADE LOADS V = 20 m/sec, θ = 86.46°, $\phi \approx 90°$.

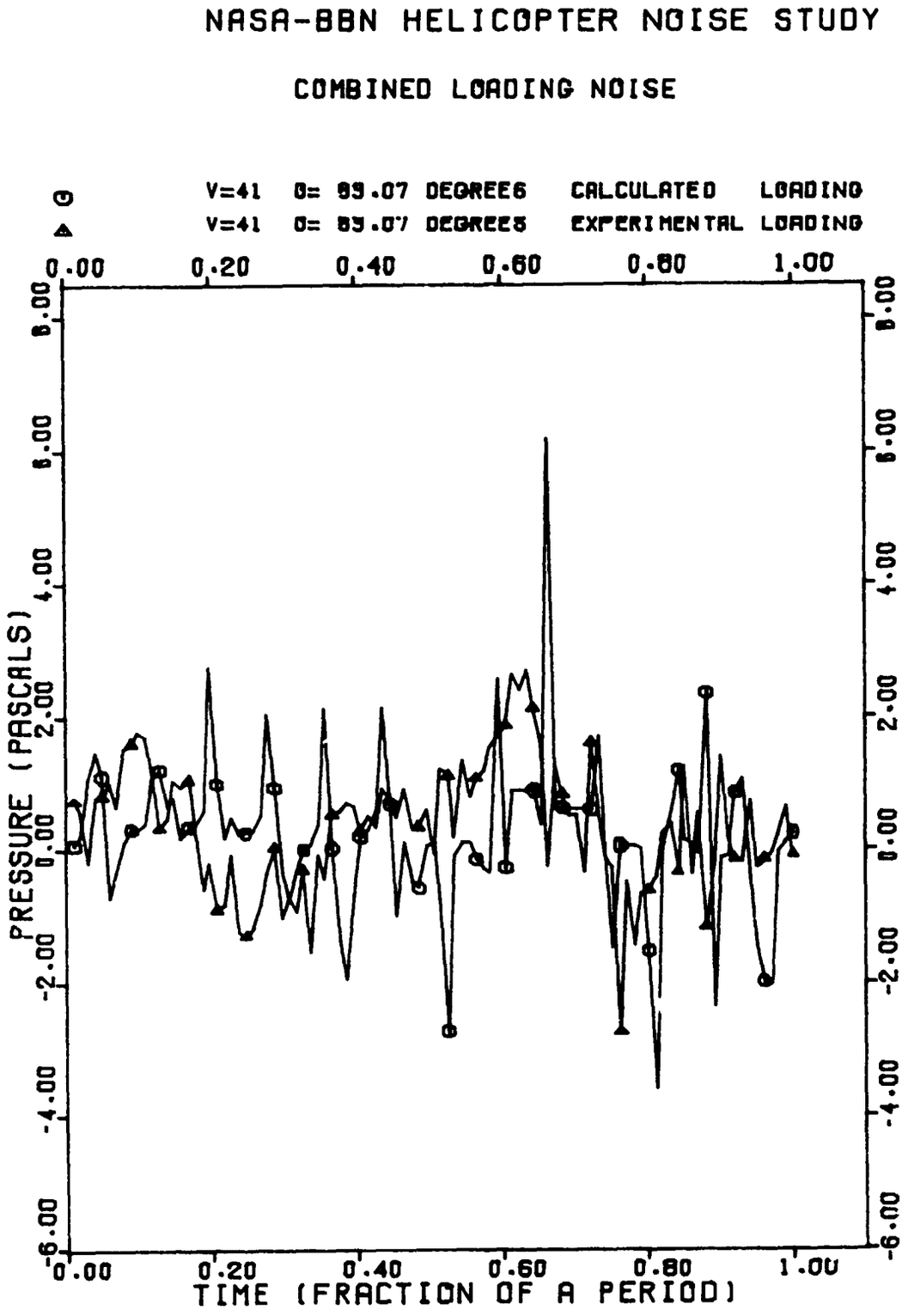

FIG. A11. COMBINED LOADING NOISE CALCULATED FROM MEASURED AND THEORETICAL BLADE LOADS V = 41 m/sec, $\theta = 83.07°$, $\phi \approx 90°$.

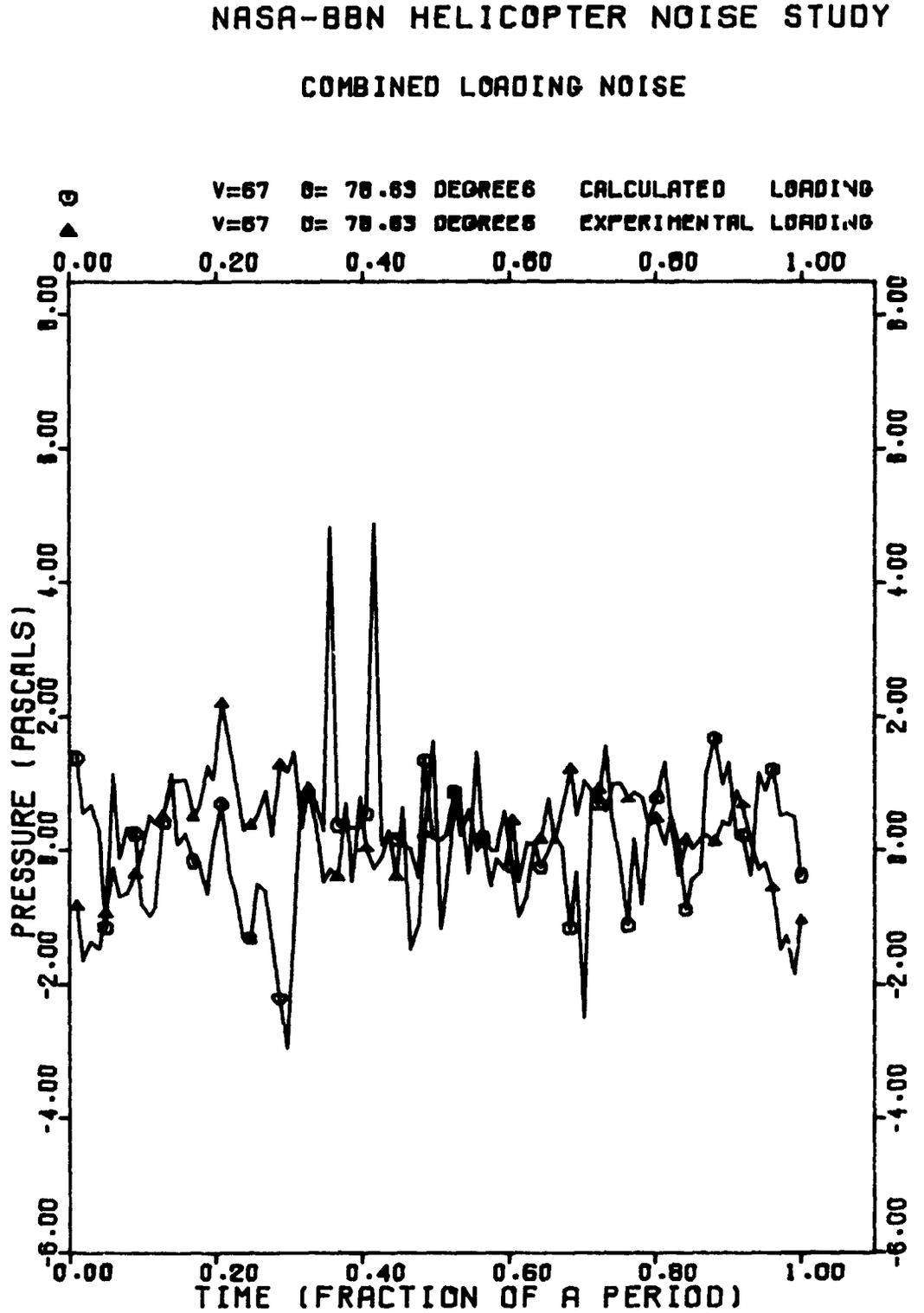

FIG. A12. COMBINED LOADING NOISE CALCULATED FROM MEASURED AND THEORETICAL BLADE LOADS V = 67 m/sec, θ = 78.63°, $\phi \approx 90°$.

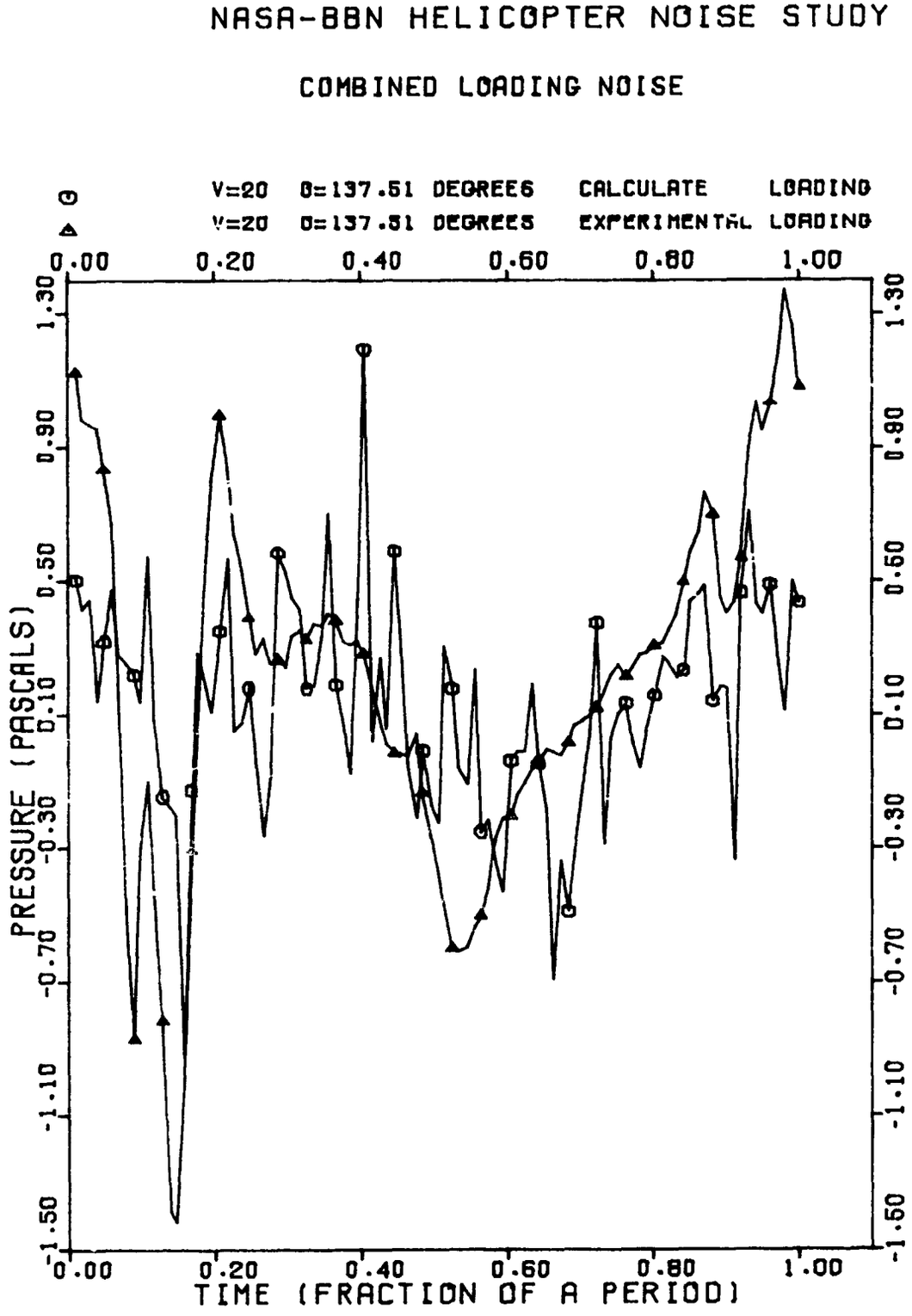

FIG. A13. COMBINED LOADING NOISE CALCULATED FROM MEASURED AND THEORETICAL BLADE LOADS V = 20 m/sec, θ = 137.51°, $\phi \approx 140°$.

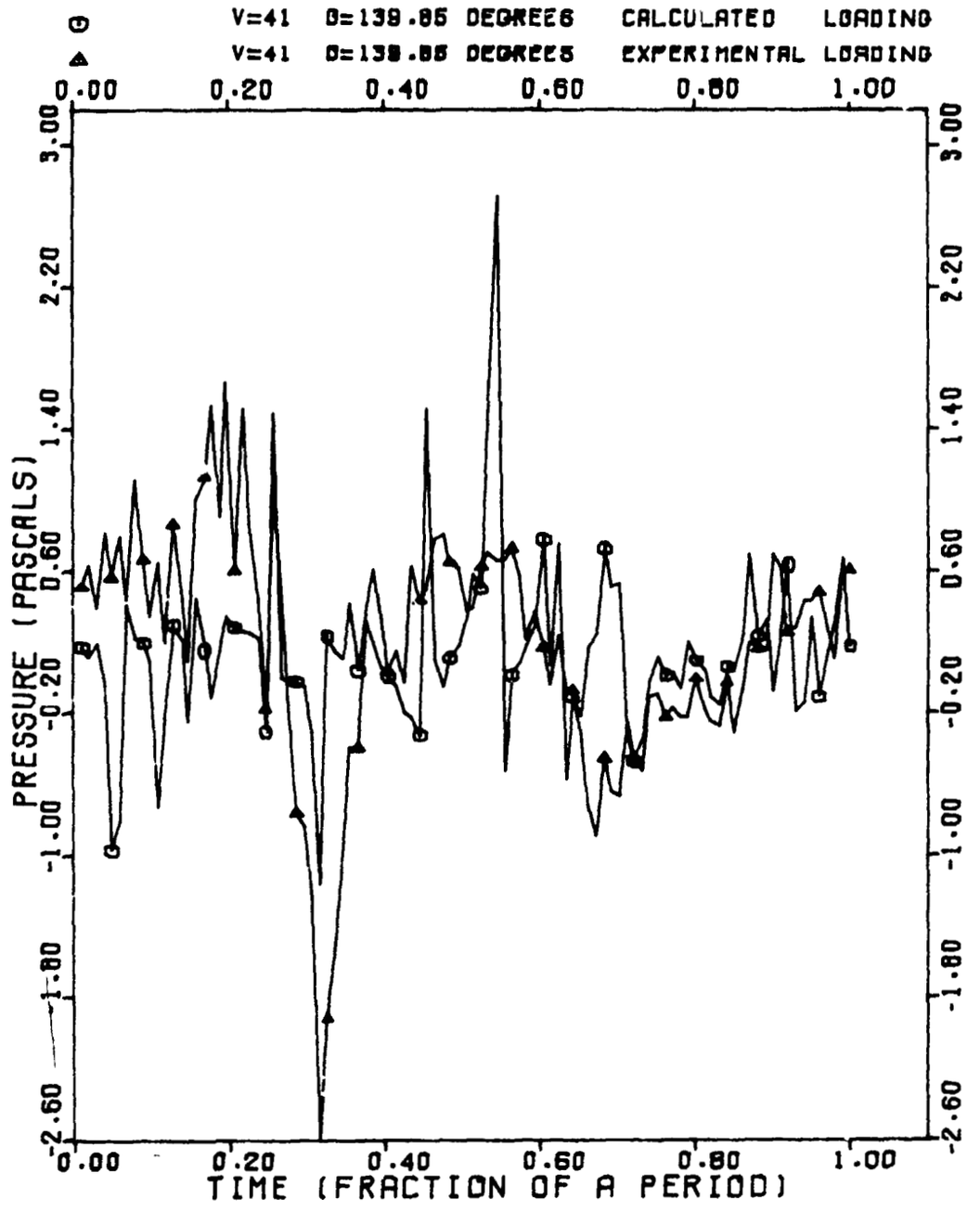

FIG. A14. COMBINED LOADING NOISE CALCULATED FROM MEASURED AND THEORETICAL BLADE LOADS V = 41 m/sec, θ = 139.85°, $\phi \approx 140°$.

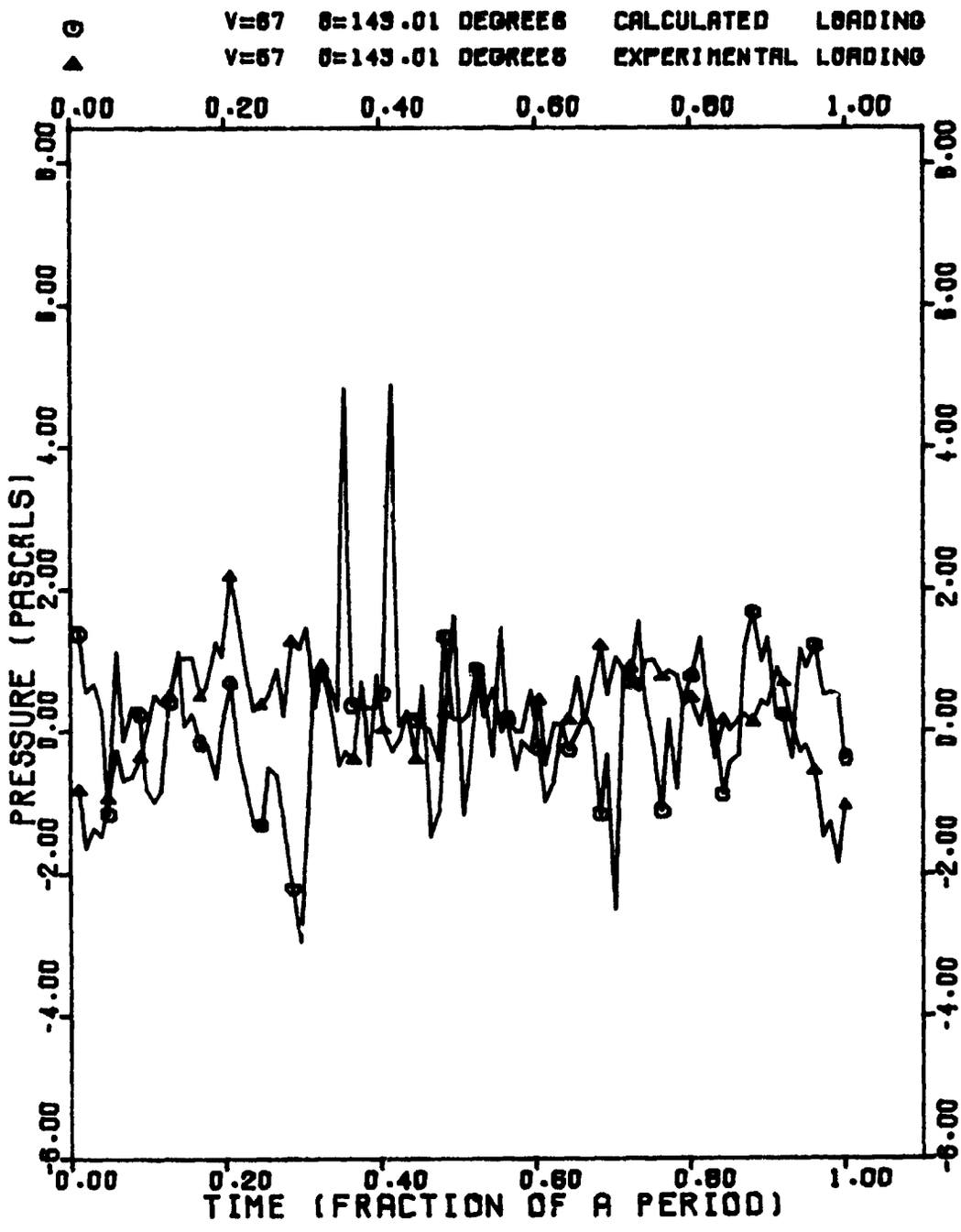

FIG. A15. COMBINED LOADING NOISE CALCULATED FROM MEASURED AND THEORETICAL BLADE LOADS V = 67 m/sec, θ = 143.01°, $\phi \approx 140°$.

APPENDIX B: COMPARISONS OF MEASURED NARROWBAND SPECTRA TO CALCULATIONS BASED ON MEASURED AND THEORETICAL BLADE LOADS

Figure B1 to B12 present the narrowband spectral analysis of the data. These analyses were computed at BBN from copies of the Bell acoustic data tapes. On each plot, two angles are listed: ϕ gives the helicopter location when the sound is detected, θ gives the helicopter location when the sound was emitted. The figures are organized by the observation angle $\phi \approx 10°$, 17°, 45°, and 90°. At each observation angle, data for 20, 41, and 67 m/sec are presented. The frequency domain of each spectra is from 0 to 200 Hz, with the sole exception of Fig. B15 which has a domain of 0 to 1000 Hz.

The spectra are computed by centering a two-second interval about the appropriate point on the data tape and fast Fourier transforming the segment. This implies a bandwidth of 1/2 Hz, which yields approximately 20 frequency bins per blade passage period. This procedure is necessary to avoid overlap between adjacent harmonics. It is adequate when the helicopter is moving slow and close to the horizon. However, the procedure is less accurate when the helicopter moves faster or approaches the overhead position. The reason is that the azimuthal location of the helicopter changes by a large amount in two seconds under these conditions. In this study, the only place where helicopter motion in a two-second interval is especially large is at the $\phi \approx 90°$ overhead point.

A better way to proceed is to select a time interval equal to one Doppler shifted blade passing period:

$$Dt = (1-M \cos\theta) \cdot T \quad ,$$

where T is the period in the helicopter frame of reference. In this fashion, the smallest possible time increment is selected. In this study, $T \approx 0.1$ sec, hence the change in the angular position of the vehicle is negligible. This procedure requires a variable bandwidth analyzer which was unavailable at the time of analysis. An alternate procedure is to digitize the analog data tapes and perform a similar analysis on the computer.

One more note on the spectra is in order. For the 20 m/sec case for $\phi \approx 10°$ and 17° (Figs. B1 and B4), a 6 dB error is believed to have been made in producing the spectra. This error could have been made by neglecting to record the setting of a 6 dB amplifier located between the tape deck and spectrum analyzer. The error was discovered by logarithmically adding the energy in each harmonic and noticing that the total energy exceeding the energy tabulated by Bell in an independent analysis. This error, of course, could be checked by analyzing the data tapes once again. Rather than incur this extra cost, alternate graphs are presented which are believed to be accurate, with the appropriate reduction of 6 dB from the initial measurement.

On each of the spectra, three computations are presented:

- spectra from calculated loads in a free field (open squares)
- spectra from measured loads in a free field (open circles)
- spectra calculated loads including ground reflection (closed circles).

The first comments concern the spectra from calculated loads including ground effect; the best estimate of the sound field. Components are organized first by observation angle and then by velocity.

At the shallowest observation angle, $\phi \approx 10°$, the spectra is predicted well (Figs. B1 to B3). There is good agreement at nearly all harmonics. At 20 m/sec, the calculated level per harmonic decays more rapidly with increasing harmonic number than at 41 and 67 m/sec in good agreement with the measured data. At 41 and 67 m/sec, the predictions are accurate at the high order harmonics, but inaccurate for the first few harmonics. One possibility for the error is the neglect of forces parallel to the blade chord. These forces are most important when the observation is made in the disk plane.

Similar observations are true at $\phi \approx 17°$ (Figs. B4 to B6). The amplitude decrease with increasing frequency is more rapid at 20 m/sec than at 41 or 67 m/sec. Again the theory predicted this effect. At 20 m/sec, the theory is accurate at all frequencies. At 41 and 67 m/sec, the theory is accurate at high frequencies; at low frequencies predictions are lower than the measured amplitudes.

At $\phi \approx 45°$, the results change (Figs. B7 to B9). The theory predicts the observed amplitude accurately at all frequencies except those frequencies approximately equal to 100 Hz. At frequencies near 100 Hz, the hard ground assumption implies nearly complete destructive interference (Fig. B10). This effect is not observed. This is due, in part, to the incorrect representation of the ground impedance. Also, the assumption that the atmosphere is quiescent neglects the random phase shifts that are caused by sound propagation through atmospheric fluctuation. This fluctuation-induced pnase shifts between the reflected and direct signal paths make complete destructive interference impossible. Hence, the large discrepancy between measurement and theory at frequencies near 100 Hz.

When the helicopter is overhead, $\phi \approx 90°$, the theory and measurement disagree and the errors are not systematic (Figs. B10 to B12). The discrepancy is due to an inaccurate measurement. The source of the error in the measurement of the spectra is the change in the location of the helicopter in the time it takes to compute the spectra.

Figures B13 and B14 give the change in the azimuthal location of the helicopter in a given time interval. In Fig. B13, the time interval is 2 sec; which is the time interval used to measure narrowband spectra with a bandwidth of 1/2 Hz. The only time in which the changes in helicopter location is large is when the helicopter is approximately overhead. As the helicopter moves faster, the change in location gets larger. In Fig. B13, the time interval is 1/2 sec; which is the time interval used to measure the OASPL. For this time interval, the change in location of the helicopter is small.

Our next comments concern the differences between the spectra computed from the calculated loads and those computed from the measured loads. The agreement is best at shallow observation angles and high forward speeds, and worst when the helicopter is overhead or when it moves slow.

There are two factors which influence the sound field:

- rotor geometry and motion
- blade loading.

The relative influence of these factors determine the correlation between acoustic predictions proceeding from theoretical and

measured loads. When rotor geometry and motion predominate, as they do at high forward speed and shallow observation angles, the two predictions agree. When blade loading has the greatest influence, as it does at low forward speed and observations near the rotor axis, the two predictions disagree. The discrepancy means that acoustical calculations using theoretical loads are not accurate enough to predict flyover noise levels.

In Fig. B15, the relative influence of main rotor and tail rotor is documented. Below 250 Hz, the main rotor dominates the spectra. Between 250 and 750 Hz, the tail rotor dominates the spectra. Above 750 Hz, no structure is seen. This observation is important because the tail rotor dominates the spectra in the frequency range where the A-weighting procedure compensates for the low harmonic amplitudes. This means any helicopter noise prediction scheme for helicopter certification studies should also include a detailed consideration of the tail rotor noise.

Note that the prediction of OASPL (Figs. 11 to 13) considers only the influence of the main rotor. This procedure is accurate because A-weighting is not used to evaluate OASPL. Inspection of Figs. B1 to B12 and B15 reveals that the main rotor noise is always greater than the tail rotor noise.

TABLE B1

V(m/sec)	20		41		67	
Approximate Observation Angle ϕ	θ	Fig.	θ	Fig.	θ	Fig.
10°	8.46	B1	8.80	B2	8.05	B3
17°	17.65	B4	15.05	B5	13.36	B6
45°	42.49	B7	40.06	B8	36.99	B9
90°	86.46	B10	83.07	B11	78.63	B12

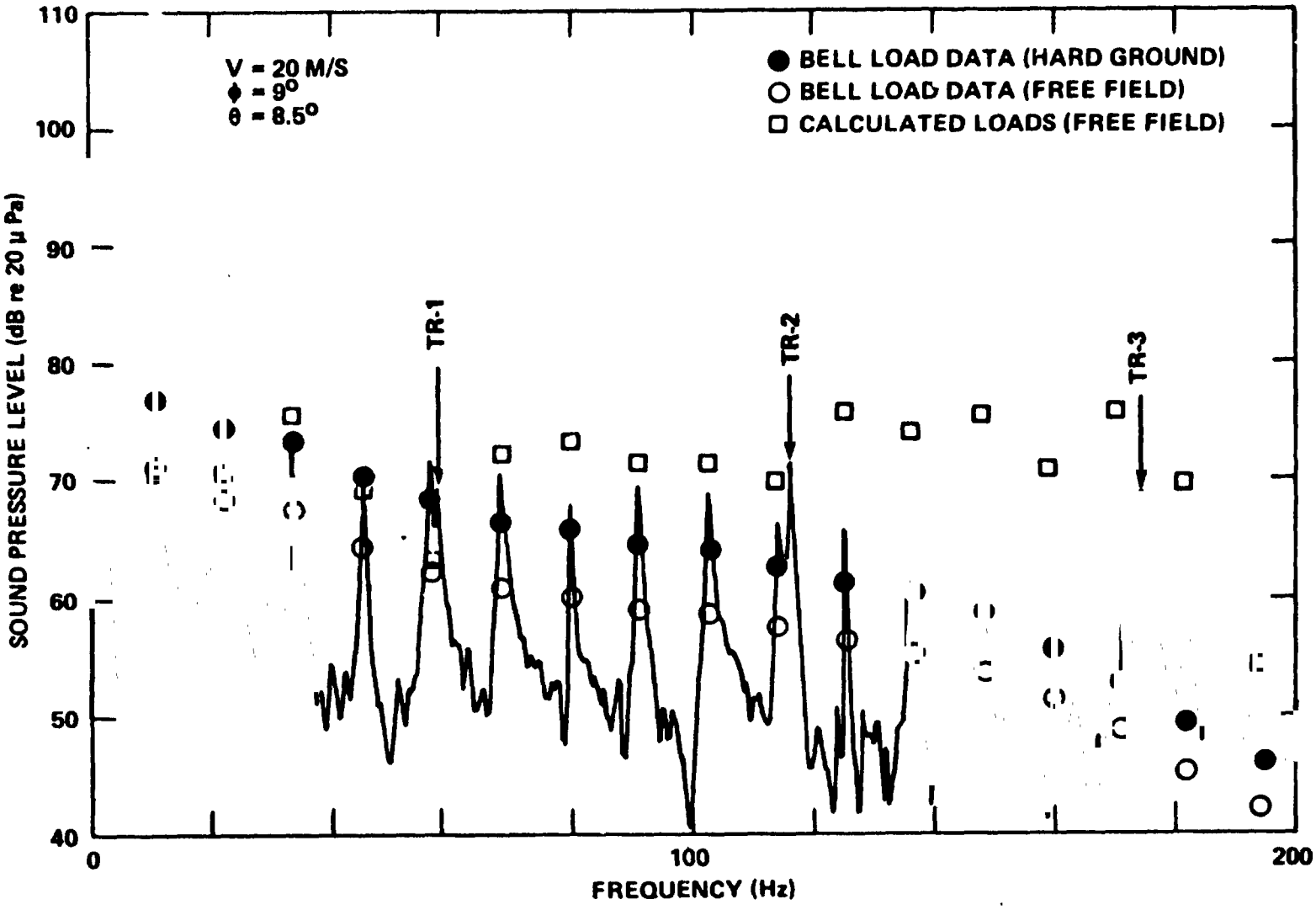

FIG. B1 THEORETICAL VS MEASURED NARROW BAND SPECTRA
V = 20 M/SEC $\phi \approx 10^{o}$

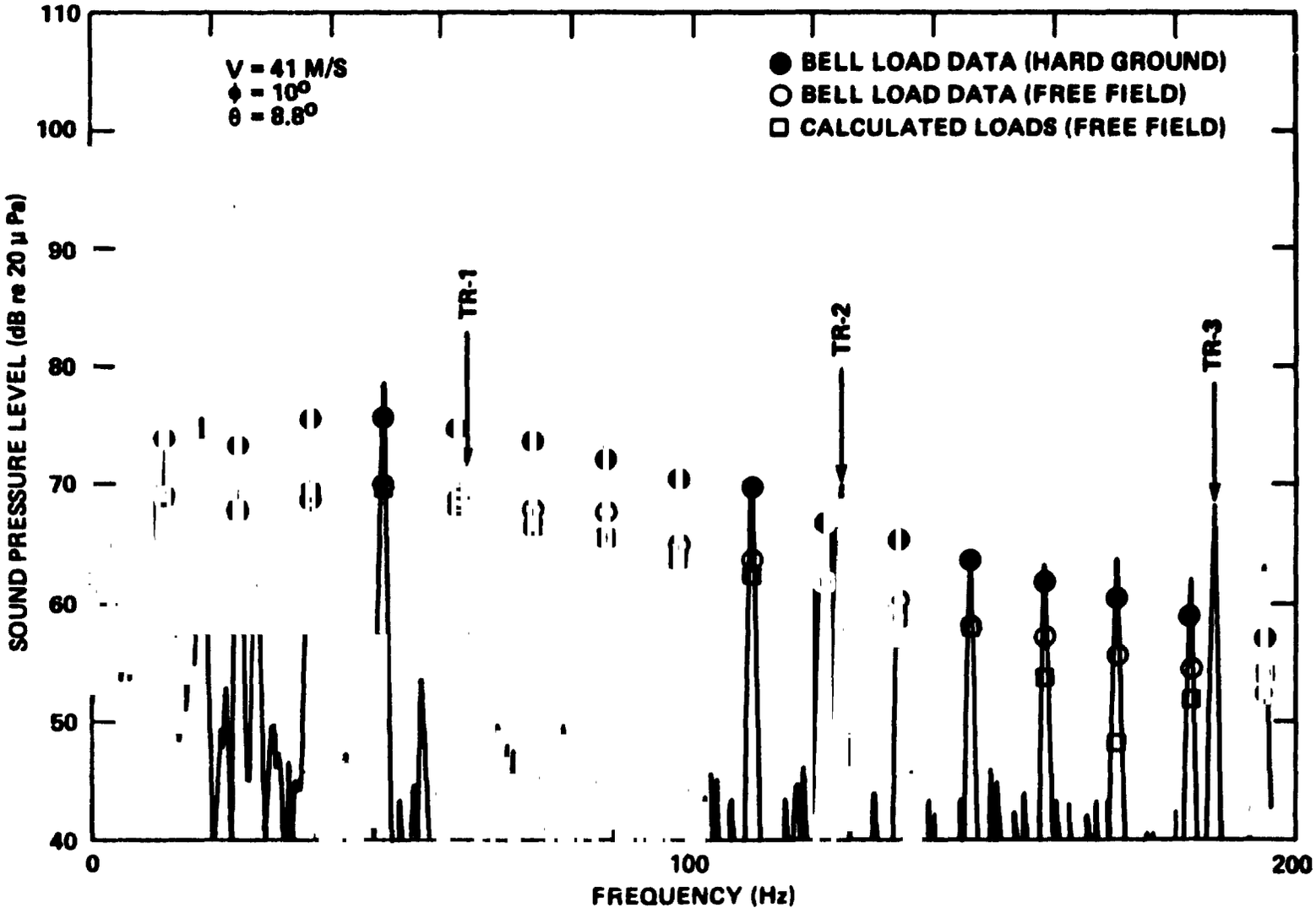

FIG. B2. THEORETICAL VS MEASURED NARROW BAND SPECTRA
V = 41 M/SEC $\phi \approx 10^{o}$

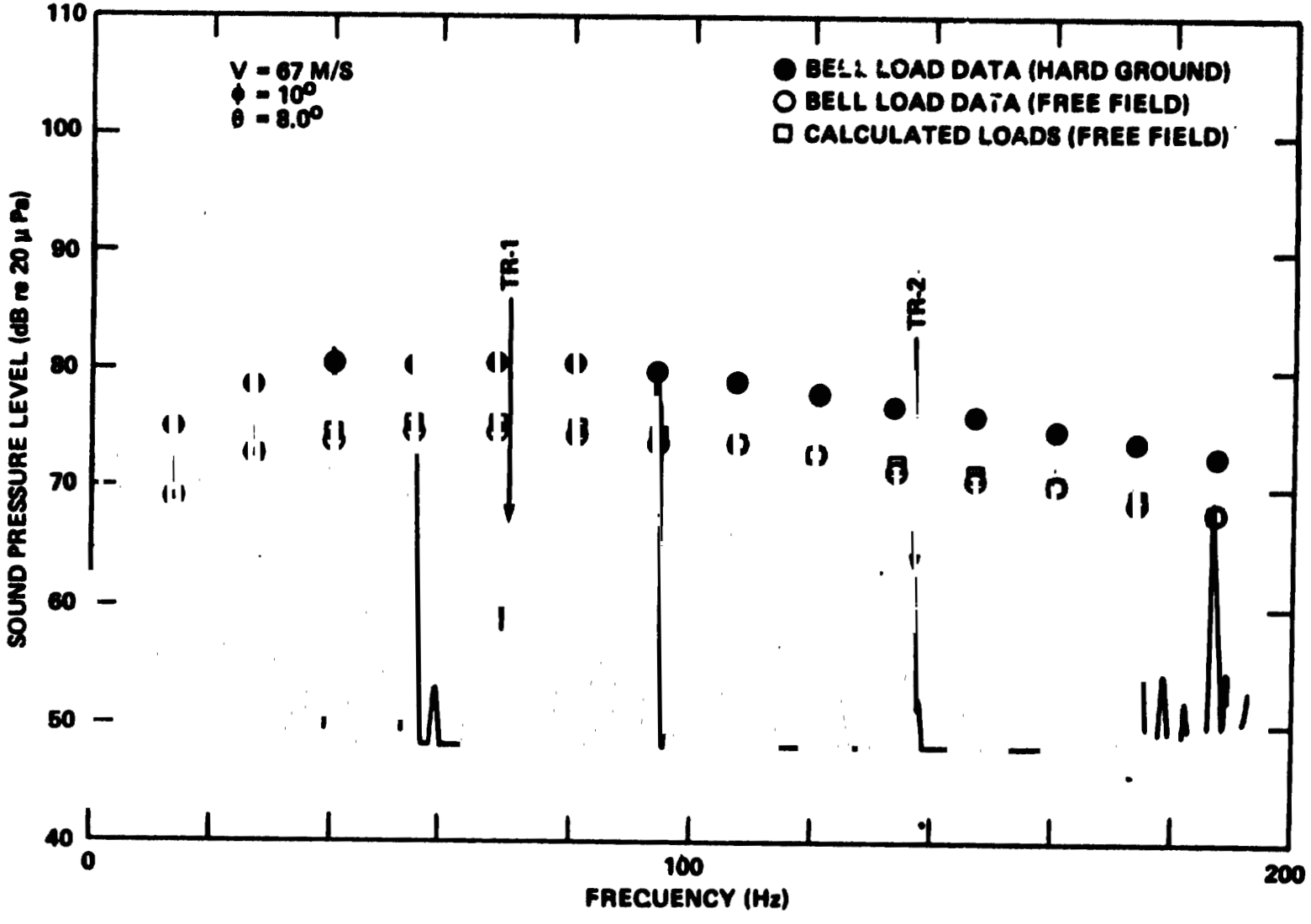

FIG. B3 THEORETICAL VS MEASURED NARROW BAND SPECTRA
V = 67 M/SEC $\phi \approx 10^{o}$

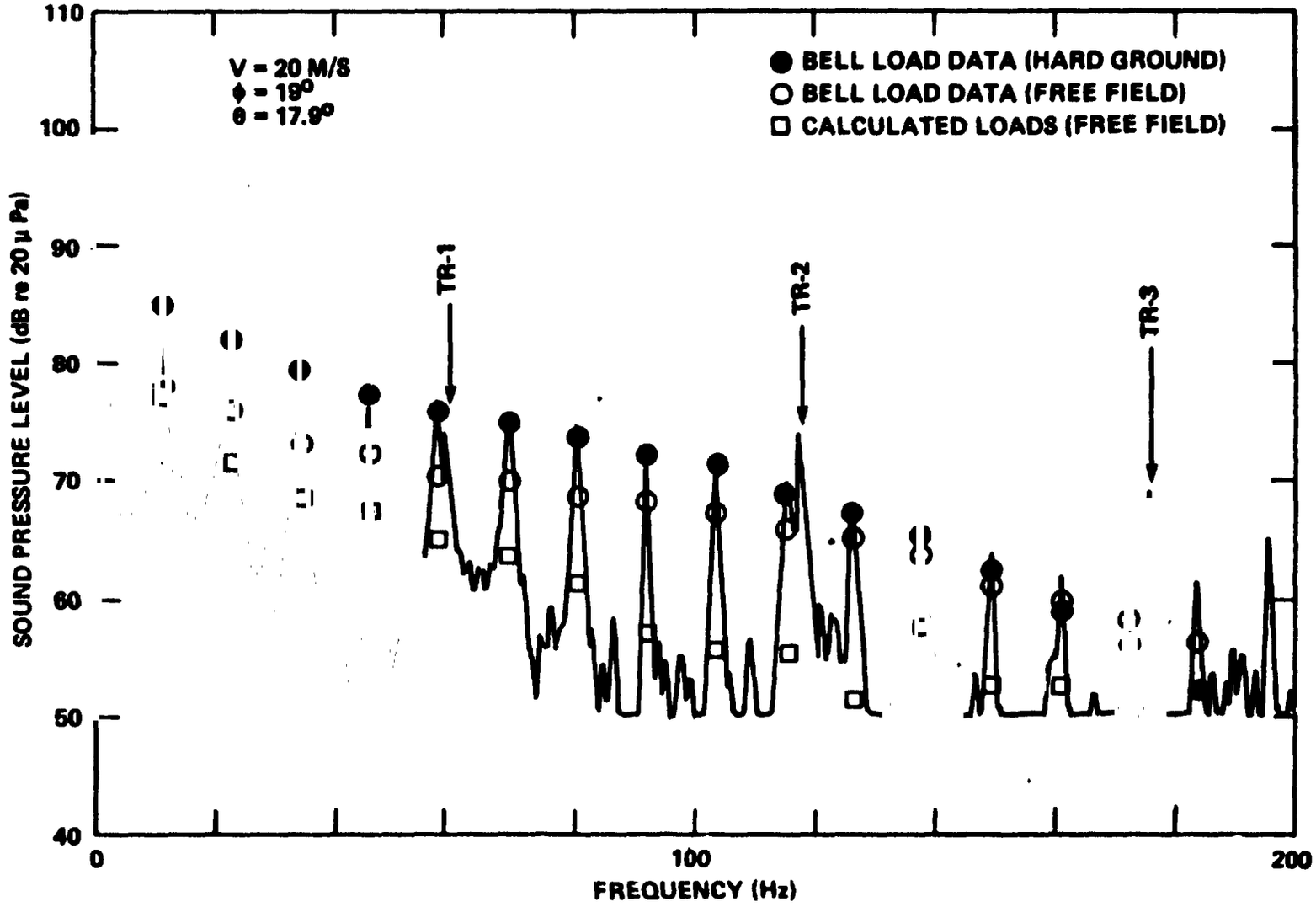

FIG. B4 THEORETICAL VS MEASURED NARROW BAND SPECTRA
V = 20 M/SEC $\phi \approx 17^{\circ}$

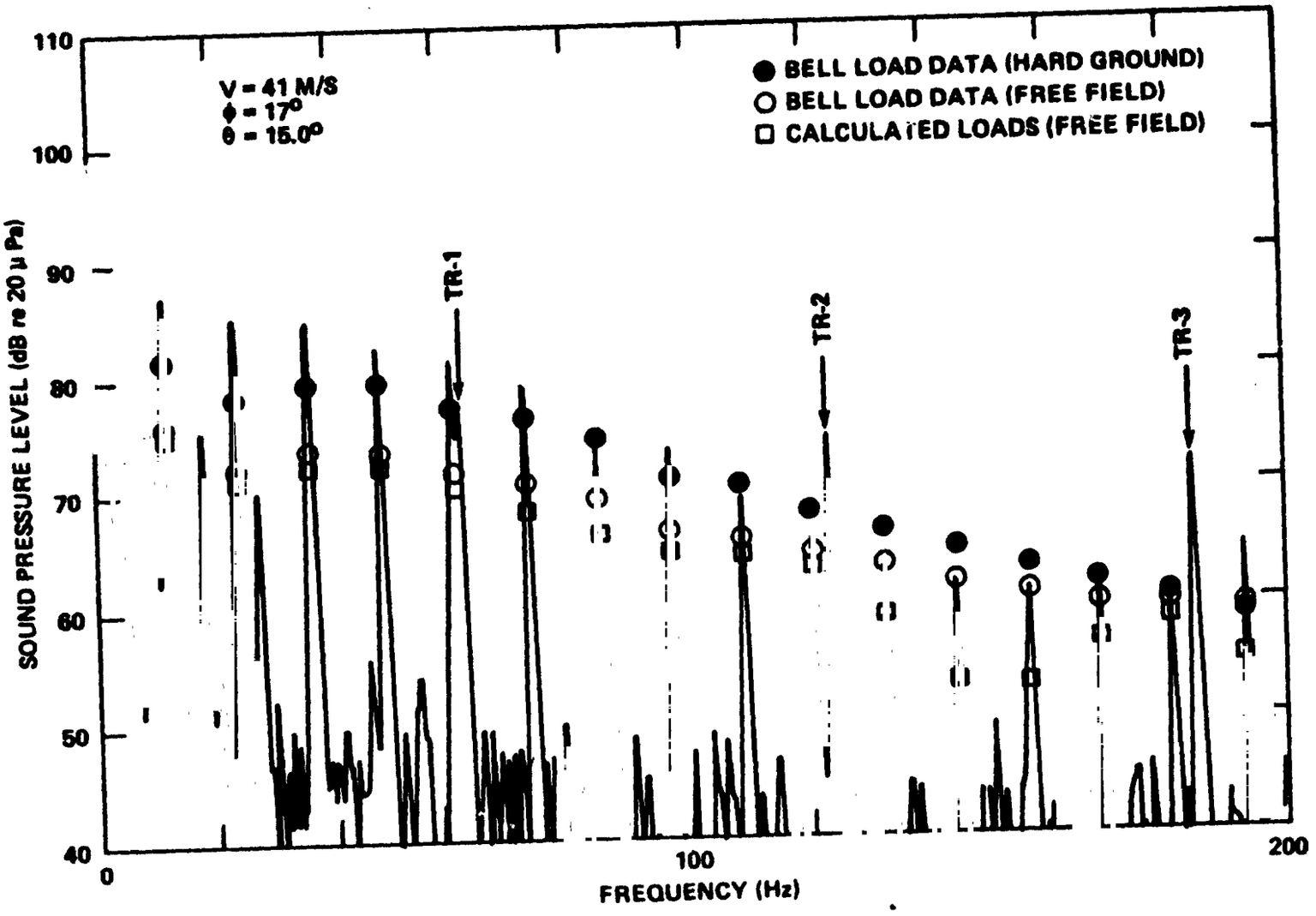

FIG. B5 THEORETICAL VS MEASURED NARROW BAND SPECTRA
V = 41 M/SEC $\phi \simeq 17^{o}$

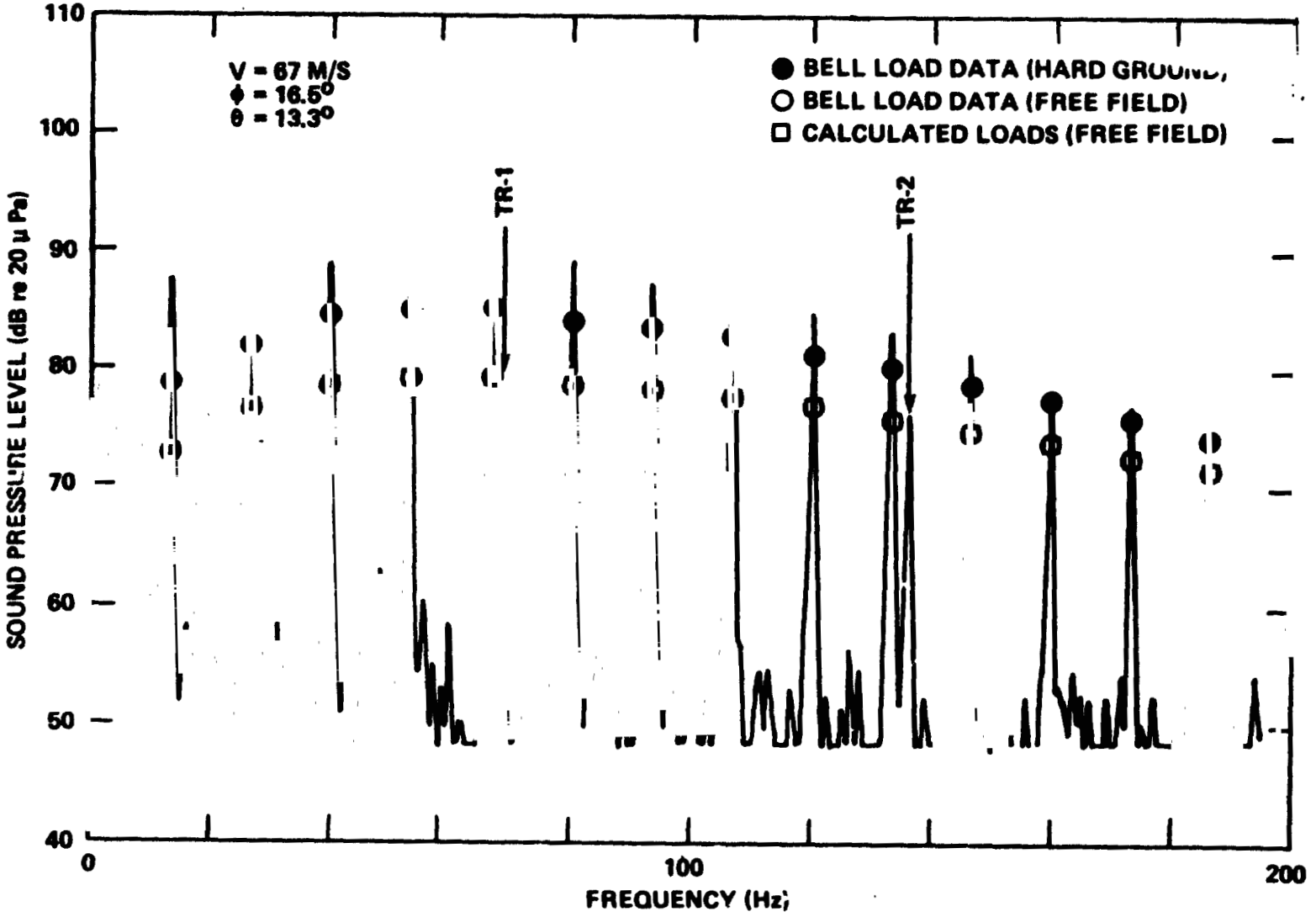

FIG. B6 THEORETICAL VS MEASURED NARROW BAND SPECTRA
V = 67 M/SEC $\phi \simeq 17^{o}$

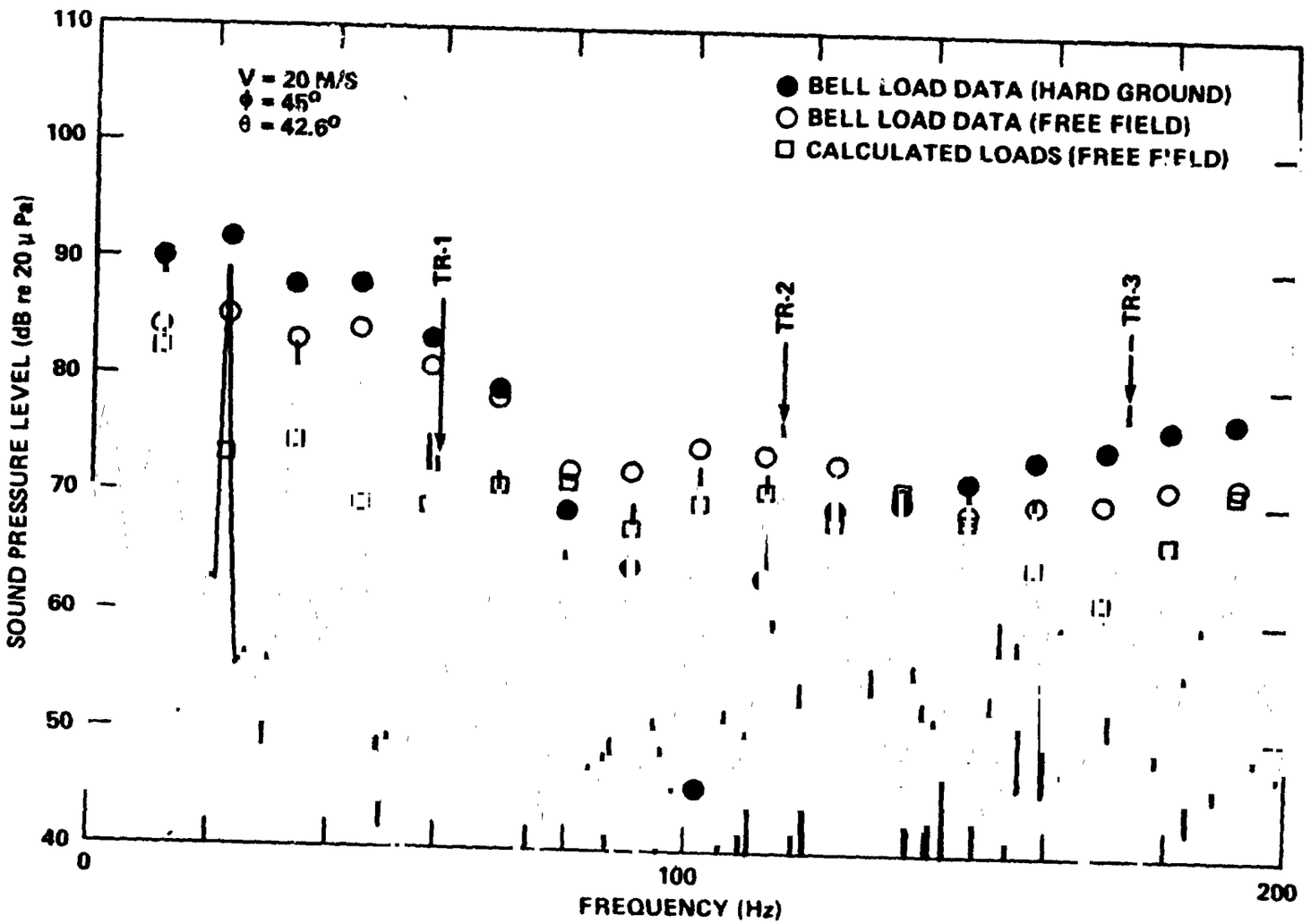

FIG. B7 THEORETICAL VS MEASURED NARROW BAND SPECTRA
V = 20 M/SEC $\phi \simeq 45^{o}$

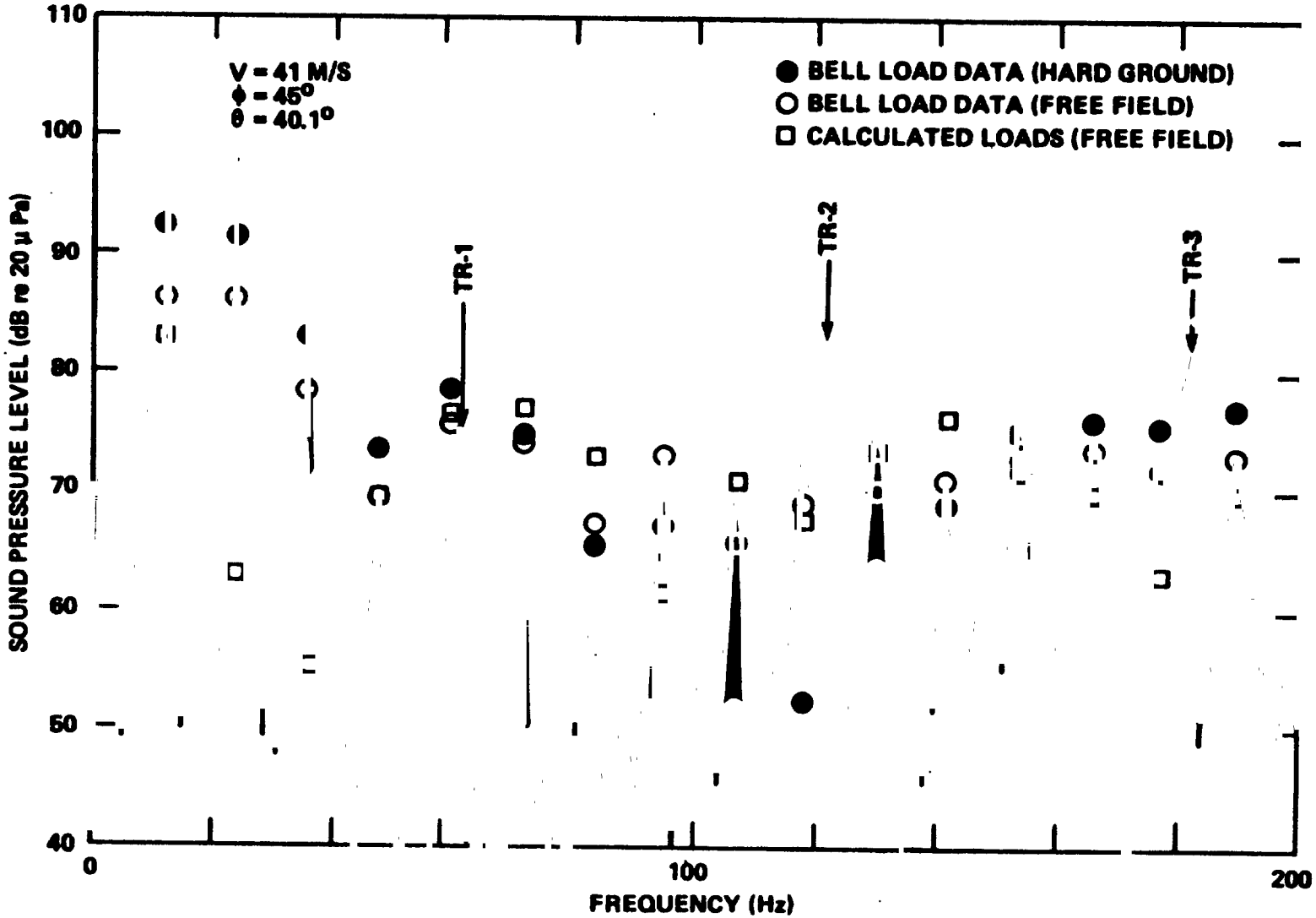

FIG. B8 THEORETICAL VS MEASURED NARROW BAND SPECTRA
V = 41 M/SEC $\phi \approx 45^{o}$

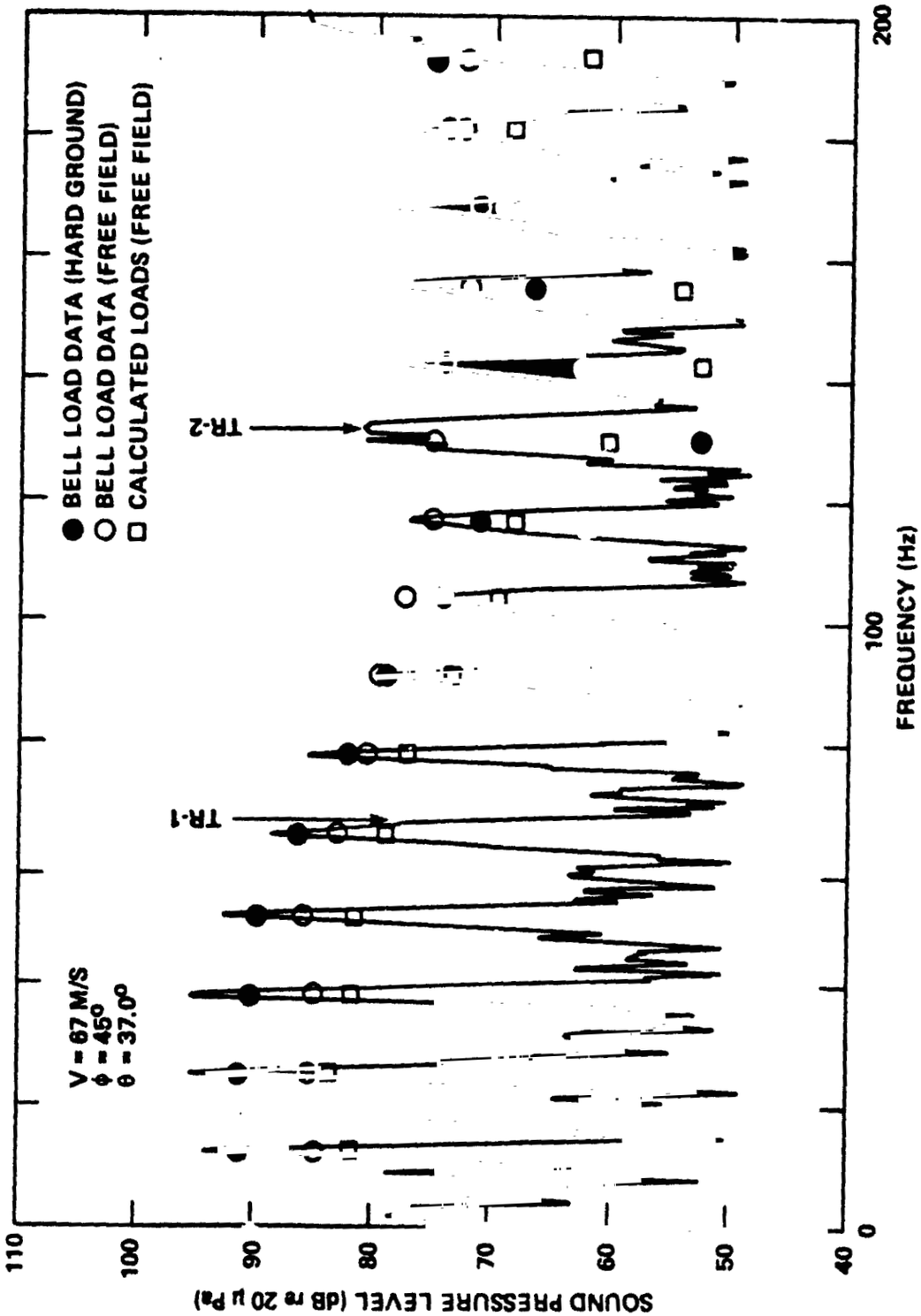

FIG. B9. THEORETICAL VS MEASURED NARROW BAND SPECTRA
V = 67 M/SEC ϕ ≈45°

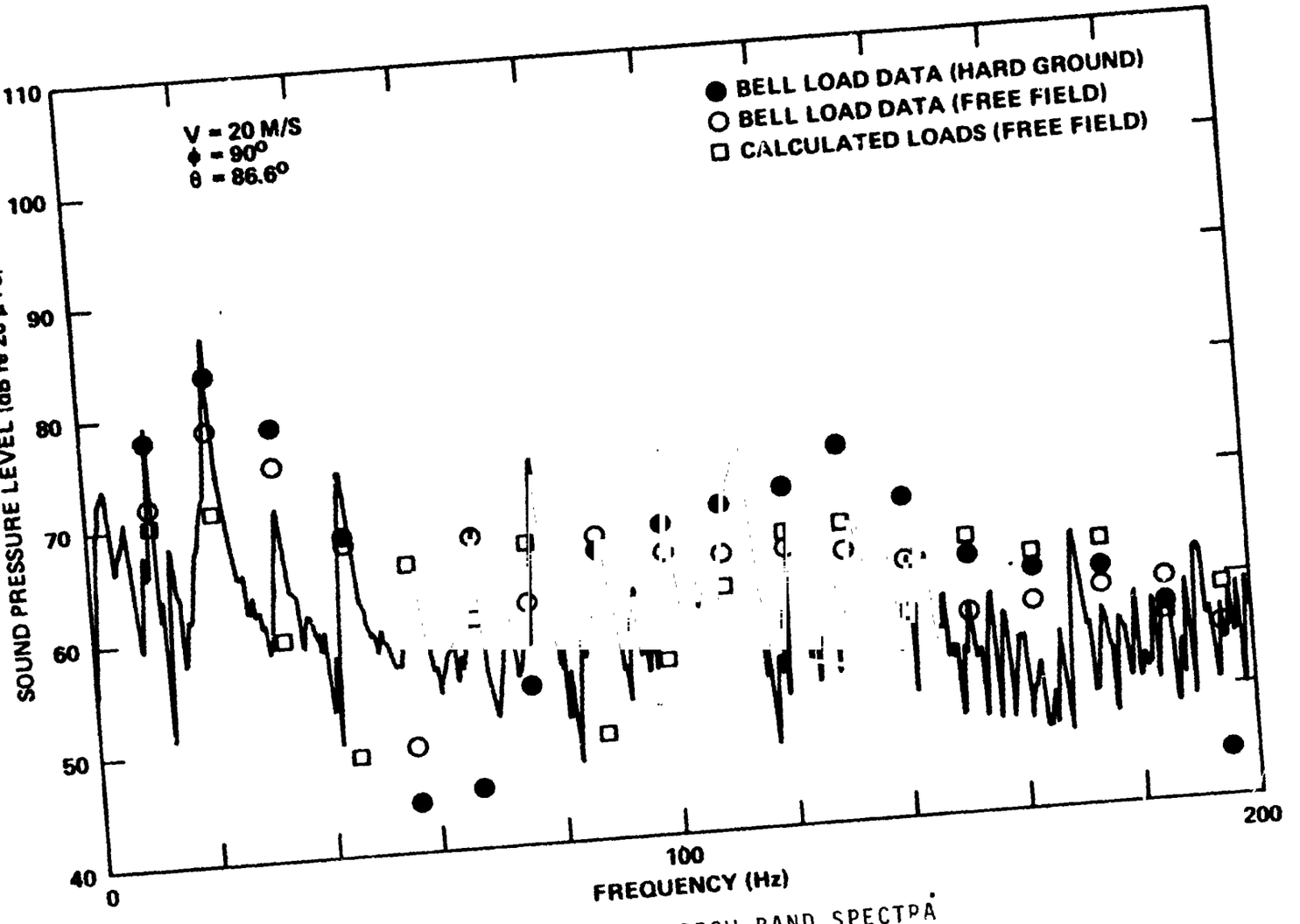

FIG. B10. THEORETICAL VS MEASURED NARROW BAND SPECTRA
V = 20 M/SEC $\phi \approx 90^{o}$

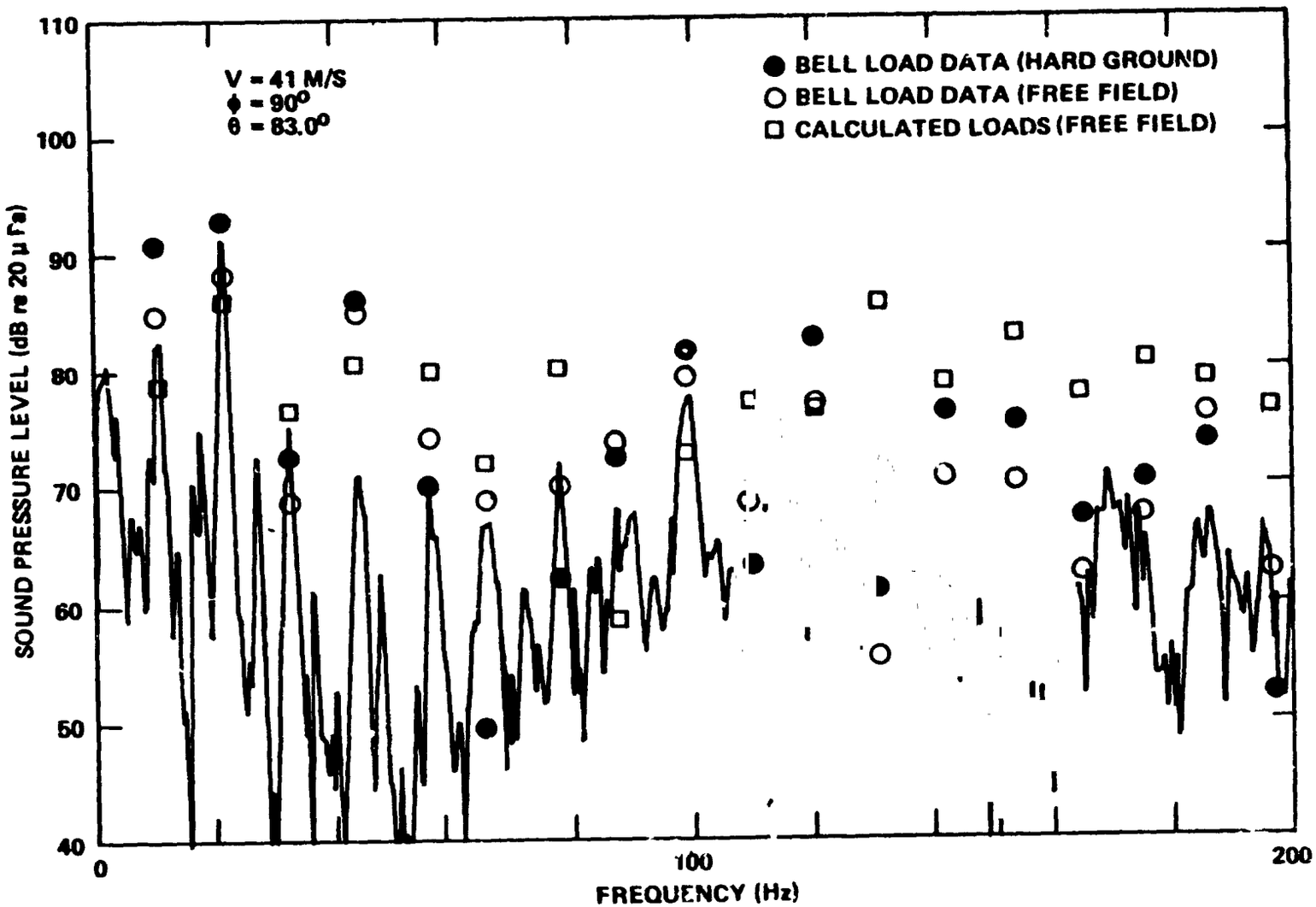

FIG. B11. THEORETICAL VS MEASURED NARROW BAND SPECTRA
V = 41 M/SEC $\phi \approx 90^{o}$

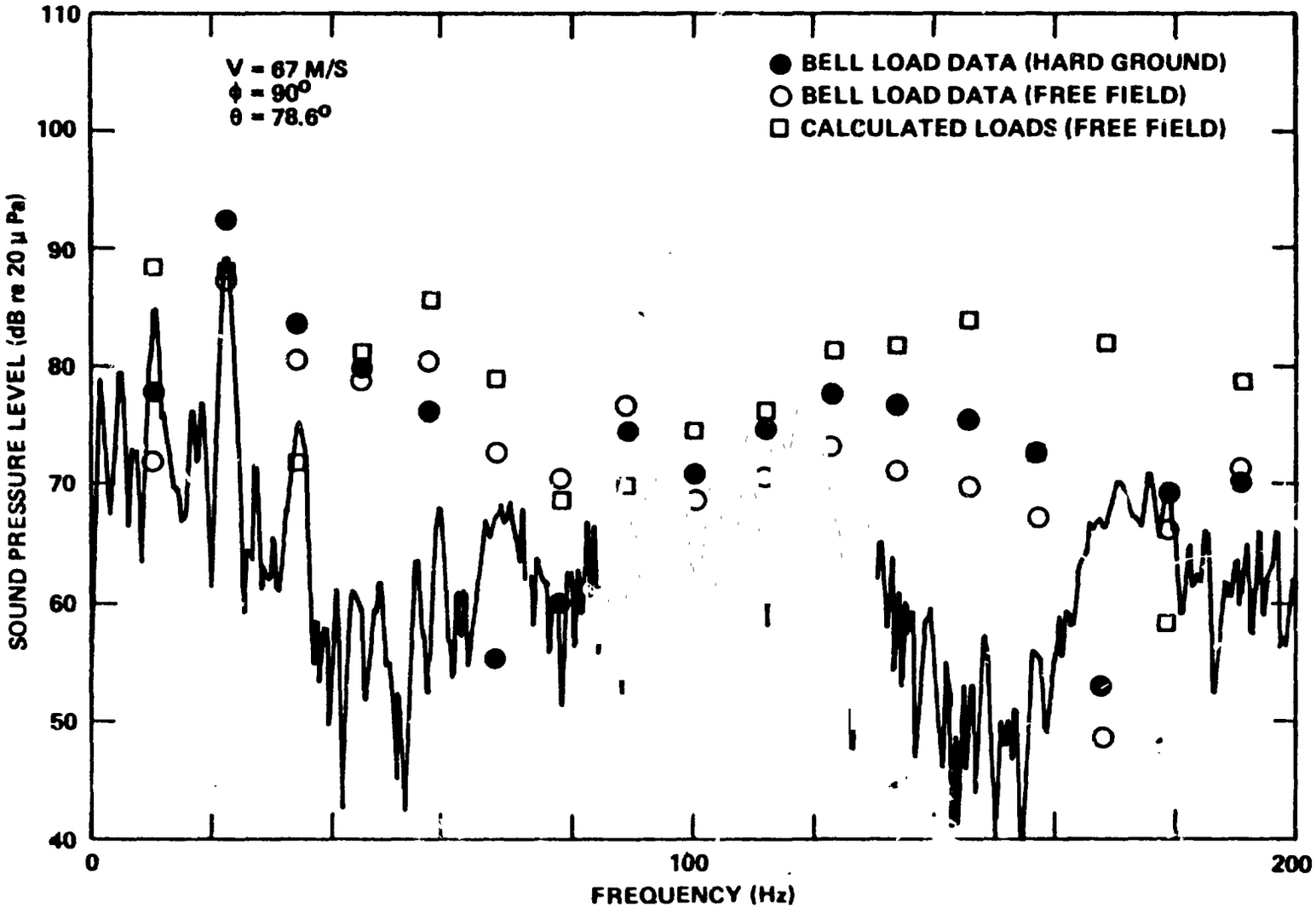

FIG. B12. THEORETICAL VS MEASURED NARROW BAND SPECTRA
V = 67 M/SEC ϕ ≈90°

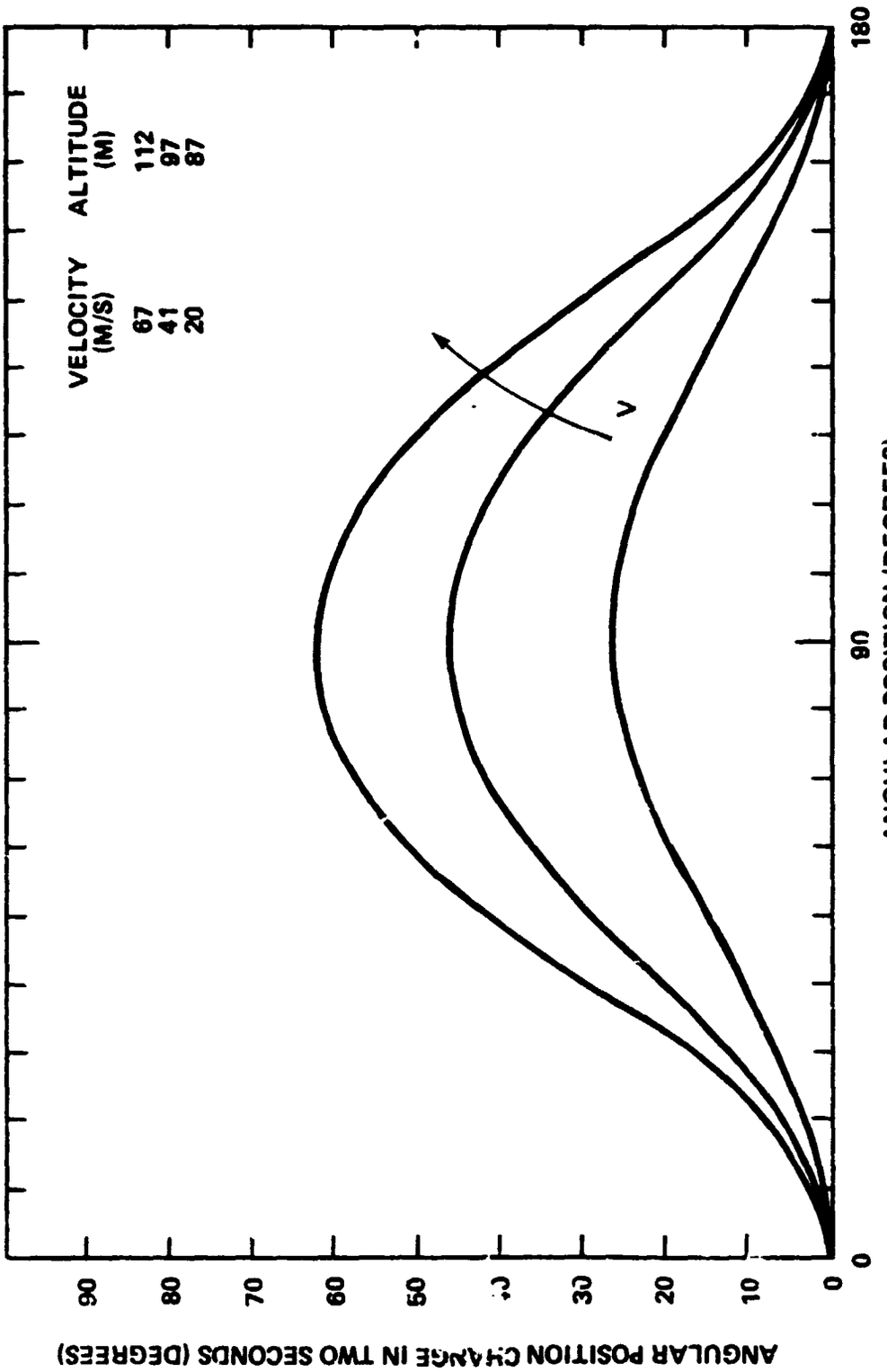

FIG. B13. ANGULAR CHANGE IN HELICOPTER LOCATION IN A 2 SEC INTERVAL

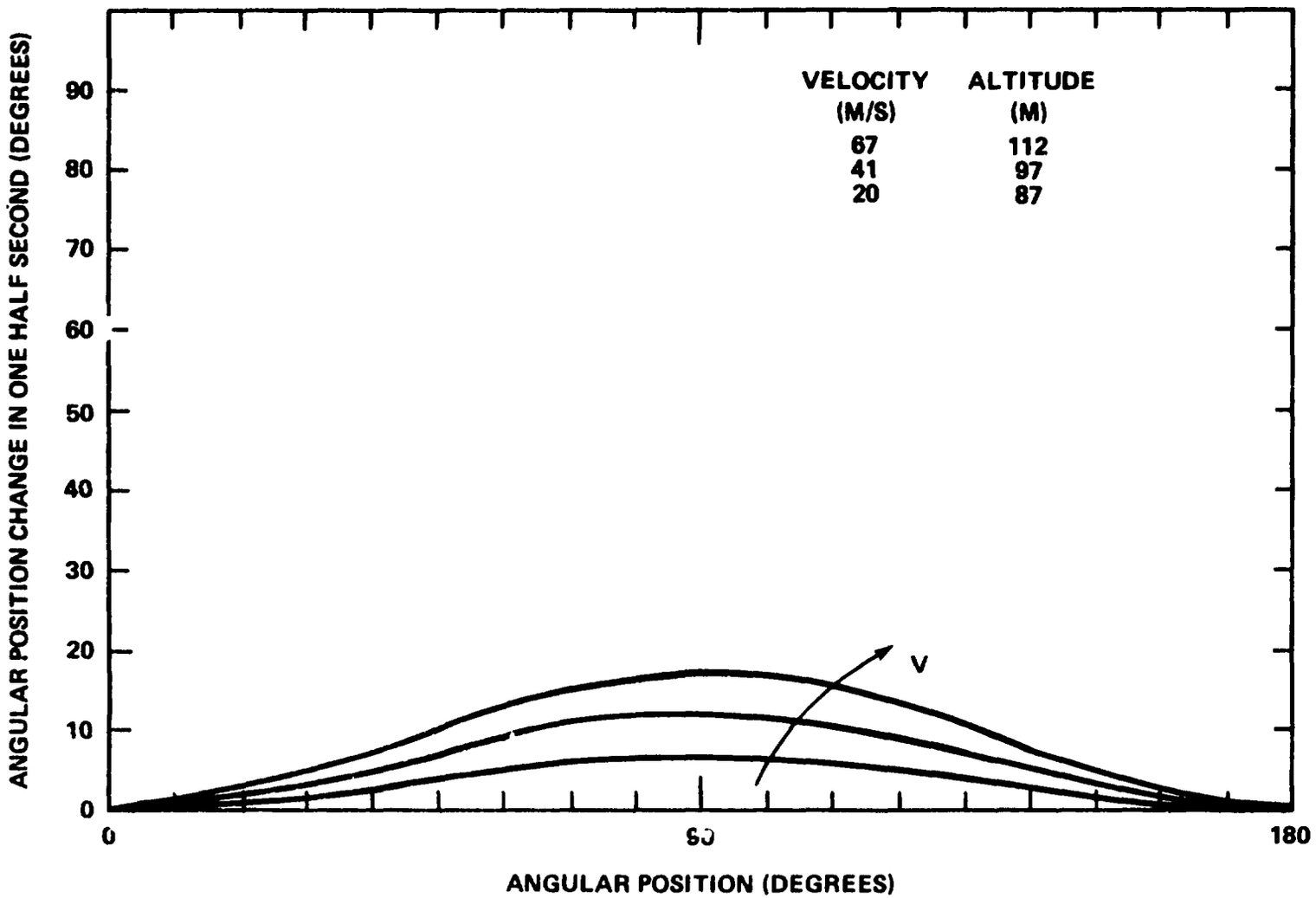

FIG.B14. ANGULAR CHANGE IN HELICOPTER LOCATION IN A 1/2 SEC INTERVAL

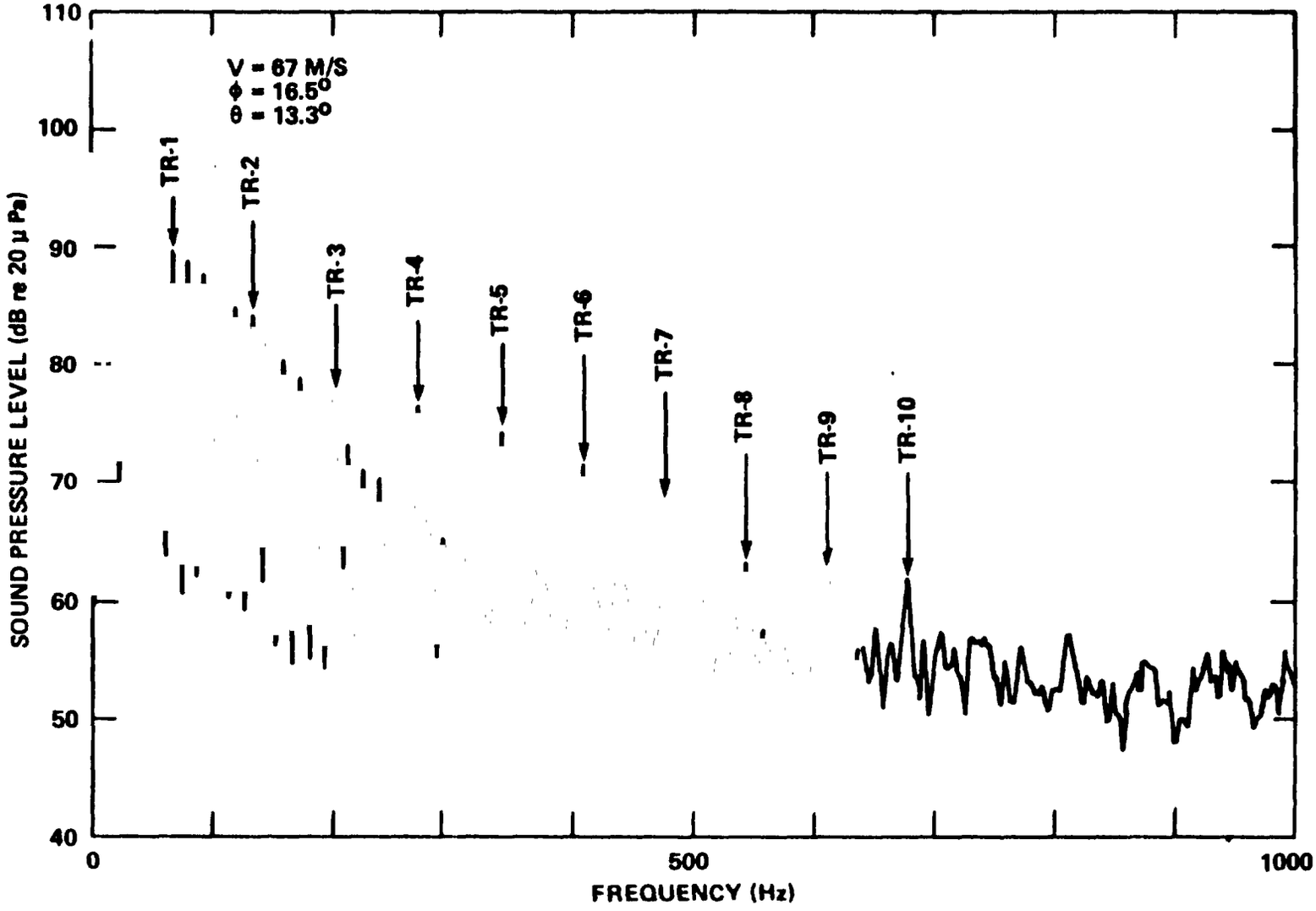

FIG. B15. TAIL ROTOR AND MAIN ROTOR SPECTRA